

# Semi-Implicit Functional Gradient Flow

Shiyue Zhang<sup>\*†</sup>      Ziheng Cheng<sup>\*‡</sup>      Cheng Zhang<sup>§</sup>

## Abstract

Particle-based variational inference methods (ParVIs) use non-parametric variational families represented by particles to approximate the target distribution according to the kernelized Wasserstein gradient flow for the Kullback-Leibler (KL) divergence. Recent works introduce functional gradient flows to substitute the kernel for better flexibility. However, the deterministic updating mechanism may suffer from limited exploration and require expensive repetitive runs for new samples. In this paper, we propose Semi-Implicit Functional Gradient flow (SIFG), a functional gradient ParVI method that uses perturbed particles as the approximation family. The corresponding functional gradient flow, which can be estimated via denoising score matching, exhibits strong theoretical convergence guarantee. We also present an adaptive version of our method to automatically choose the suitable noise magnitude. Extensive experiments demonstrate the effectiveness and efficiency of the proposed framework on both simulated and real data problems.

## 1 Introduction

Bayesian inference aims to efficiently estimate and sample from unnormalized posterior distribution to model complex data and reason under uncertainty, which is a fundamental and challenging task in modern machine learning. Typical methods including Markov Chain Monte Carlo (MCMC) and Variational Inference (VI), have been developed to address the intractability of the target distribution. By reformulating the inference problem into an optimization problem, VI seeks to find an approximation within a specific distribution family that minimizes the Kullback-Leibler (KL) divergence to the posterior [Jordan et al., 1999; Wainwright and Jordan, 2008; Blei et al.,

---

\*Equal contribution.

†Peking University. Email: zhangshiyue@stu.pku.edu.cn

‡University of California, Berkeley. Email: ziheng\_cheng@berkeley.edu

§Peking University. Email: chengzhang@math.pku.edu.cn

2016]. Though VI allows fast training and feasible scaling to large datasets when equipped with efficient optimization algorithms, the main restriction is that the choice of variational distribution family may limit its approximation power. On the other hand, MCMC simulates a Markov chain to directly draw samples from the posterior [Duane et al., 1987; Robert and Stramer, 2002; Neal, 2011; Welling and Teh, 2011; Chen et al., 2014]. While being asymptotically unbiased, MCMC often takes a long time to converge, and it is also difficult to access the convergence.

Recently, there has been a growing interest in the gradient flow formulation of both MCMC and VI, leading to the development of particle-based variational inference methods (ParVIs) that tend to combine the best of both worlds [Liu and Wang, 2016; Chen et al., 2018; Liu et al., 2019; di Langosco et al., 2021; Fan et al., 2022; Alvarez-Melis et al., 2022]. In ParVIs, the approximating distribution is represented by a set of particles, which are iteratively updated by minimizing the KL divergence to the posterior according to the gradient flow. This non-parametric nature significantly improves the flexibility of ParVIs upon classical VIs, and the interaction between particles also makes ParVIs more particle-efficient than MCMCs. One of the most prominent particle based VI method is Stein Variational Gradient Descent (SVGD) [Liu and Wang, 2016]. It updates the particles by simulating the gradient flows of the KL divergence within a reproducing kernel Hilbert space (RKHS), where the gradient flows have a tractable form [Liu, 2017; Chewi et al., 2020]. However, the performance of SVGD heavily relies on the choice of the kernel function and the quadratic computational complexity of the kernel matrix also hinders practical usage of a large number of particles.

To address these issues, functional gradient flow methods have been proposed to expand the function class for gradient flow approximation [Hu et al., 2018; Grathwohl et al., 2020; di Langosco et al., 2021; Dong et al., 2023; Cheng et al., 2023]. By leveraging the more general neural network induced functional gradients, these approaches have presented improved performance over vanilla SVGD while not requiring expensive kernel computation. However, due to the deterministic updating mechanism, current approaches often struggle with limited exploration and can encounter mode collapse when dealing with non-convex multi-modal distributions. Additionally, multiple runs are required to generate different sets of samples, which adds to the computational burden.

In this work, we propose Semi-Implicit Functional Gradient flow (SIFG), a novel ParVI method that leverages a semi-implicit variational family, represented by perturbed particles, to approximate the target distribution. The injected Gaussian noise enhances the algorithm’s exploration, and the corresponding Wasserstein gradient flow is efficiently estimated via denoising score matching, which scales well in high-dimensional settings. Additionally, this added stochasticity enables the

generation of diverse samples on the fly, addressing a common limitation of ParVI methods due to their deterministic nature. We provide a theoretical convergence guarantee of SIFG, which is a non-trivial generalization of the convergence theory of variational inference with mixture gaussians with fixed variance [Huix et al., 2024]. We also propose an adaptive procedure that can automatically adjust the noise magnitude, balancing between sample accuracy and diversity. Extensive numerical experiments on both simulated and real data sets are conducted to demonstrate the advantage of our method over existing ParVI methods.

## 2 Related Works

Existing functional gradient methods for ParVIs mainly focus on designing more expressive function space for the velocity field in gradient flow dynamics than the Reproducing Kernel Hilbert Space (RKHS). di Langosco et al. [2021] proposed to use neural networks rather than kernels to approximate the optimal velocity with  $L_2$  regularization. Dong et al. [2023] and Cheng et al. [2023] generalize the regularizer to quadratic and  $L_p$  functions. While functional gradient flow methods enjoy more flexibility because of the expansion from RKHS to neural networks, the updating mechanisms therein remain deterministic. This may lead to lack of exploration ability and sample diversity: the particles may get stuck at local modes for complex distributions, and only a single set of samples could be obtained from one run.

Previous works explore the possibilities of utilizing broader variational family for variational inference, including gaussian-based variational inference and incorporating semi-implicit variational family with particle gradient flows. Lambert et al. [2022] and Diao et al. [2023] proposed convergence analysis for non-degenerate gaussian distribution family. Furthermore, Huix et al. [2024] presented the theoretical analysis for gaussian mixture family. In this work, we generalize and improve the convergence theory from gaussian mixture family to the general semi-implicit family. Lim and Johansen [2024] proposed to assist Semi-Implicit Variational Inference (SIVI) with particle guidance by alternatively updating the variational parameters and the particles representing the semi-implicit distribution through minimizing the regularized KL objective. The simulation of particles requires a McKean–Vlasov SDE which is similar to the Langevin diffusion. As a functional gradient method, our method do not use Langevin type of particle updating, and selecting the noise to be Gaussian enables us to directly use the KL divergence as the objective.

### 3 Background

**Notations** Throughout this paper, we use  $z \in \mathbb{R}^d$  to denote the particle samples before perturbation, and we use  $x \in \mathbb{R}^d$  to denote the perturbed particle samples. Let  $\mathcal{P}(\mathbb{R}^d)$  denote all the probability distributions on  $\mathbb{R}^d$  that are absolute continuous with respect to the Lebesgue measure. We do not distinguish a probabilistic measure with its density function. Let  $\|\cdot\|$  be the standard Euclidean norm of a vector and the operator norm of a matrix or high-dimensional tensor. We denote the inner product in  $\mathbb{R}^d$  (or  $L^2(\mathbb{R}^d)$ ) and a certain Hilbert space  $\mathcal{H}$  by  $\langle \cdot, \cdot \rangle$  and  $\langle \cdot, \cdot \rangle_{\mathcal{H}}$ , respectively. We use  $\frac{\delta \mathcal{F}}{\delta \mu}$  to denote the first variation of the functional  $\mathcal{F}$ , and we use  $\nabla_{W_2} \mathcal{F} := \nabla \frac{\delta \mathcal{F}}{\delta \mu}$  to denote the Wasserstein-2 gradient of  $\mathcal{F}$ .

#### 3.1 Functional Gradient Flow

Let  $\pi$  be the target distribution we wish to sample from. Particle-based variational inference methods aim to minimize the KL divergence between the distribution  $\mu$  represented by a set of particles and the target distribution  $\pi$ ,

$$\mu^* := \arg \min_{\mu \in \mathcal{Q}} D_{\text{KL}}(\mu \|\pi), \quad (3.1)$$

where  $\mathcal{Q}$  is the space of probability measures. Starting from the initial distribution  $\mu_0$  and the initial particle  $z_0 \sim \mu_0$ , we update the particle  $z_t$  following  $dz_t = v_t(z_t)dt$ , where  $v_t$  is the velocity field at time  $t$ . The distribution  $\mu_t$  of  $z_t$  follows the continuity equation  $\partial_t \mu_t + \nabla \cdot (\mu_t v_t) = 0$ , and the KL divergence decreases with the following rate:

$$\frac{d}{dt} D_{\text{KL}}(\mu_t \|\pi) = -\mathbb{E}_{\mu_t} \langle \nabla \log \frac{\pi}{\mu_t}, v_t \rangle. \quad (3.2)$$

The optimal  $v_t$  in a Hilbert space  $\mathcal{H}$  is the minimizer of the following objective:

$$\min_{v_t \in \mathcal{H}} -\mathbb{E}_{\mu_t} \langle \nabla \log \frac{\pi}{\mu_t}, v_t \rangle + \frac{1}{2} \|v_t\|_{\mathcal{H}}^2. \quad (3.3)$$

SVGd [Liu and Wang, 2016] chooses  $\mathcal{H}$  to be the Reproducing Kernel Hilbert Space with kernel  $k(\cdot, \cdot)$ , and the optimal velocity field takes the following form

$$v_t^*(\cdot) = \mathbb{E}_{\mu} [k(\cdot, x) \nabla \log \pi(x) + \nabla_x k(\cdot, x)], \quad (3.4)$$

Functional gradient flow methods define  $\mathcal{H}$  to be  $\mathcal{L}^2(\mu_t)$  and parameterize  $v_t$  as a neural network. By Stein's identity, objective (3.3) has a tractable form

$$v_t^* = \arg \min_{v \in \mathcal{F}} \mathbb{E}_{\mu_t} \left[ -\langle \nabla \log \pi, v \rangle - \nabla \cdot v + \frac{1}{2} \|v\|^2 \right], \quad (3.5)$$

where  $\mathcal{F}$  is the neural network family.

## 3.2 Semi-implicit Variational Inference

In SIVI, the variational family takes a hierarchical architecture:

$$x|z \sim q_\phi(x|z), z \sim \mu_\xi(z), \mu_\phi(x) = \int q_\phi(x|z)\mu_\xi(z)dz \quad (3.6)$$

where  $\phi, \xi$  are model parameters. Variants of semi-implicit variational inference fit the model parameters in different ways, including maximizing the surrogate evidence lower bound (ELBO) [Yin and Zhou, 2018], using unbiased gradient estimator of the exact ELBO [Titsias and Ruiz, 2019], minimizing Fisher divergence [Yu and Zhang, 2023] and minimizing KSD [Cheng et al., 2024].

## 4 Proposed Method

### 4.1 Semi-implicit Particle-based Variational Family

Suppose  $\mu_t$  is the current particle distribution at time  $t$ . Inspired from the semi-implicit structure, we utilize the semi-implicit version of the current distribution  $\mu_t$  by injecting noise to the current particles. In this paper we focus on isotropic gaussian noise with variance  $\sigma^2$ . This leads to the following semi-implicit variational distribution  $\hat{\mu}_t$

$$\hat{\mu}_t(x) = \int q_\sigma(x|z)d\mu_t(z) \quad (4.1)$$

where  $q_\sigma(x|z) \propto e^{-\frac{\|x-z\|^2}{2\sigma^2}}$  is a gaussian transition kernel. To sample from the target distribution using the semi-implicit family, we turn to minimize the KL divergence between  $\hat{\mu}_t$  and  $\pi$ .

Following common practice in variational inference, we consider the KL divergence between the perturbed density  $\hat{\mu}_t$  and the target distribution  $\pi$ .

$$\mathcal{F}(\hat{\mu}_t) := D_{\text{KL}}(\hat{\mu}_t||\pi) = \int \log \frac{\hat{\mu}_t(x)}{\pi(x)}d\hat{\mu}_t(x) \quad (4.2)$$

### 4.2 Functional Gradient Flow

We construct a Wasserstein gradient flow that minimizes the above KL divergence. Consider the dynamics of the original particles

$$\frac{d}{dt}z_t = v_t(z_t), z_t \sim \mu_t, \quad (4.3)$$

The continuity equation is

$$\frac{d\mu_t}{dt} + \nabla \cdot (\mu_t v_t) = 0, \quad (4.4)$$

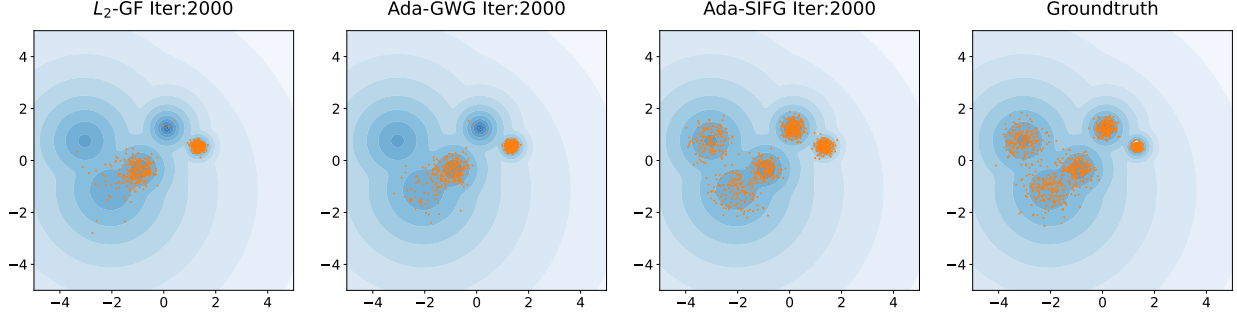


Figure 1: Comparison of sampled particles of different methods at 2000 iterations (sufficient for all methods to converge) against the ground truth samples on the 2D gaussian mixture distribution.

By the chain rule, the time derivative of the KL divergence is

$$\frac{d\mathcal{F}}{dt} = \left\langle \frac{\delta}{\delta \hat{\mu}_t} \mathcal{F}(\hat{\mu}_t), \frac{d\hat{\mu}_t}{dt} \right\rangle \quad (4.5)$$

$$= \left\langle \log \frac{\hat{\mu}_t(x)}{\pi(x)}, \int q_\sigma(x|z) \frac{d\mu_t(z)}{dt} \right\rangle \quad (4.6)$$

Plugging in the continuity equation gives

$$\frac{d\mathcal{F}}{dt} = \int \log \frac{\hat{\mu}_t(x)}{\pi(x)} \int q_\sigma(x|z) \frac{d\mu_t(z)}{dt} dx \quad (4.7)$$

$$= - \int \log \frac{\hat{\mu}_t(x)}{\pi(x)} \int q_\sigma(x|z) \nabla_z \cdot (\mu_t(z) v_t(z)) dz dx \quad (4.8)$$

$$= \int \log \frac{\hat{\mu}_t(x)}{\pi(x)} \int \nabla_z q_\sigma(x|z) \mu_t(z) v_t(z) dz dx \quad (4.9)$$

$$= \int \left[ \int \log \frac{\hat{\mu}_t(x)}{\pi(x)} \nabla_z q_\sigma(x|z) dx \right] v_t(z) \mu_t(z) dz \quad (4.10)$$

The dissipation property of the Wasserstein gradient flow states that  $\frac{d}{dt} \mathcal{F} = -\mathbb{E}_{\mu_t} \|\nabla_{W_2} \mathcal{F}\|^2$ , and the optimal velocity  $v_t^*$  is the negative of the Wasserstein gradient [Chewi et al., 2020]. From (4.10) we have

$$v_t^*(z) = - \nabla_{W_2} \mathcal{F}(\mu_t)(z) \quad (4.11)$$

$$= - \int \log \frac{\hat{\mu}_t(x)}{\pi(x)} \nabla_z q_\sigma(x|z) dx \quad (4.12)$$

$$= \int \log \frac{\hat{\mu}_t(x)}{\pi(x)} \nabla_x q_\sigma(x|z) dx \quad (4.13)$$

$$= \int \nabla \log \frac{\pi(x)}{\hat{\mu}_t(x)} q_\sigma(x|z) dx \quad (4.14)$$

$$= \mathbb{E}_{q_\sigma(x|z)} \nabla \log \frac{\pi(x)}{\hat{\mu}_t(x)} \quad (4.15)$$

where the equation of (4.13) is guaranteed by the symmetry of the gaussian transition kernel.

Following the framework of functional gradient flow, we use a neural network  $f_\gamma$  to approximate  $\nabla \log \frac{\pi(x)}{\hat{\mu}_t(x)}$  given perturbed samples  $x$ . Previous works utilize Hutchinson estimation of  $\nabla \cdot f_\gamma$  to approximate this score difference by minimizing the loss function below.

$$\mathcal{L}(\gamma) := \mathbb{E}_{\hat{\mu}_t} [\|f_\gamma\|_2^2 - \langle \nabla \log \frac{\pi}{\hat{\mu}_t}, f_\gamma \rangle] \quad (4.16)$$

$$= \mathbb{E}_{\hat{\mu}_t} [\|f_\gamma\|_2^2 - (\nabla \log \pi)^T f_\gamma - \nabla \cdot f_\gamma] \quad (4.17)$$

However, Hutchinson estimation can have large variance, especially in high dimensions. Note that we utilized the semi-implicit variational family  $\hat{\mu}_t$ , it is feasible to directly use neural network  $g_\gamma$  to estimate  $\nabla \log \hat{\mu}_t$  using denoising score matching (DSM) [Vincent, 2011]. by minimizing the loss function below:

$$\mathcal{L}(\gamma) := \mathbb{E}_{\mu_t(z)} \mathbb{E}_{q_\sigma(x|z)} [\|g_\gamma(x) - \nabla_x \log q_\sigma(x|z)\|^2] \quad (4.18)$$

$$= \mathbb{E}_{\mu_t(z)} \mathbb{E}_{q_\sigma(x|z)} [\|g_\gamma(x) + \frac{x-z}{\sigma^2}\|^2] \quad (4.19)$$

Using DSM improves the accuracy and efficiency of computing the training objective, further demonstrating the advantages of semi-implicit particle-based variational families for functional gradient computation. We call our method Semi-Implicit Functional Gradient Flow (SIFG), and summarize the overall sampling procedures in Algorithm 1.

### 4.3 Adaptively Choosing the Noise Magnitude

SIFG introduces an additional tuning parameter  $\sigma$  for balancing between sample accuracy and diversity. Increasing  $\sigma$  may improve the diversity of sample outputs, but at the same time it may also reduce the sample approximation accuracy. If we focus on achieving sample accuracy such that the KL divergence continues decaying after updating current particles, we can add a simple gradient descent procedure on  $\sigma$  according to the following gradient estimate

$$\frac{d}{d\sigma} \mathcal{F}_\sigma(\mu_t) = \mathbb{E}_{z \sim \mu_t(z), w \sim \mathcal{N}(0, I)} \nabla \log \frac{\hat{\mu}_{\sigma, t}(z + \sigma w)}{\pi(z + \sigma w)} \cdot w \quad (4.21)$$

$$\approx \mathbb{E}_{z \sim \mu_t(z), w \sim \mathcal{N}(0, I)} [f_\gamma(z + \sigma w) - \nabla \log \pi(z + \sigma w)] \cdot w \quad (4.22)$$

Please refer to the appendix A for detailed derivation. This way, we can adaptively adjust the noise level  $\sigma$  on the fly. We call this adaptive version of SIFG, Ada-SIFG. The full procedure of Ada-SIFG can be found in Algorithm 2 of the appendix A.

---

**Algorithm 1** SIFG: semi-implicit functional gradient flow

---

**Require:** Unnormalized target distribution  $\pi$ , initial particles  $\{z_0^i\}_{i=1}^n$ , initial parameter  $\gamma_0$ , iteration number  $N, N'$ , particle step size  $h$ , parameter step size  $\eta$ , noise magnitude  $\sigma$ .

**for**  $k = 0, \dots, N - 1$  **do**

Assign  $\gamma_k^0 = \gamma_k$

Obtain perturbed samples  $x_k^i = z_k^i + \epsilon_k^i$ , where  $\epsilon_k^i \sim \mathcal{N}(0, \sigma^2)$

**for**  $t = 0, \dots, N' - 1$  **do**

Compute

$$\widehat{\mathcal{L}}(\gamma) = \frac{1}{n} \sum_{i=1}^n \left\| f_\gamma(x_k^i) - \frac{x_k^i - z_k^i}{\sigma^2} \right\|^2 \quad (4.20)$$

Update  $\gamma_k^{t+1} = \gamma_k^t + \eta \nabla_\gamma \widehat{\mathcal{L}}(\gamma_k^t)$

**end for**

Update  $\gamma_{k+1} = \gamma_k^{N'}$

Update particles  $z_{k+1}^i = z_k^i + h(\nabla \log \pi(x_k^i) - f_{\gamma_{k+1}}(x_k^i))$  for  $i = 1, \dots, n$

**end for**

Obtain perturbed samples  $x_N^i = z_N^i + \epsilon_N^i$ , where  $\epsilon_N^i \sim \mathcal{N}(0, \sigma^2)$

**return** Particles  $\{x_N^i\}_{i=1}^n$

---

## 5 Theoretical Analysis

In this section, we state the main theoretical results of Algorithm 1, including convergence guarantee and sample complexity analysis.

### 5.1 Optimization Guarantees

We propose the optimization analysis of the gradient flow. Consider the discrete dynamics of the original particles

$$z_{(k+1)h} = z_{kh} + h v_k(z_{kh}), \quad (5.1)$$

and the interpolation

$$z_{(k+t)h} = z_{kh} + t h v_k(z_{kh}), \text{ for } t \in [0, 1], \quad (5.2)$$

The optimal velocity is  $v_k^*(z) = \mathbb{E}_{q_\sigma(x|z)}[\nabla \log \pi(x) - \nabla \log \hat{\mu}_{kh}(x)]$ , assume neural network parameterized  $v_k(z) = \mathbb{E}_{q_\sigma(x|z)}[\nabla \log \pi(x) - f_\gamma(x)]$ . Under the neural network approximation [Cheng



et al., 2023] and bounded assumptions with the moment condition of the particle distribution along the trajectory, we obtain the descent lemma for the gradient flow.

**Assumption 5.1.** For any  $k$ ,  $\mathbb{E}_{\hat{\mu}_{kh}} \|f_\gamma - \nabla \log \hat{\mu}_{kh}\|_2^2 \leq \varepsilon_k$ .

By triangular inequality, this assumption implies that

$$\mathbb{E}_{\mu_{kh}} \|v_k - v_k^*\|^2 = \mathbb{E}_{\mu_{kh}} \|\mathbb{E}_{q_\sigma(x|z)}(f_\gamma - \nabla \log \hat{\mu}_{kh})\|^2 \leq \varepsilon_k. \quad (5.3)$$

**Assumption 5.2.** The score of the target distribution  $\nabla \log \pi$  is L-Lipschitz, i.e. for any  $x, y \in \mathbb{R}^d$ ,  $\|\nabla \log \pi(x) - \nabla \log \pi(y)\| \leq L\|x - y\|$ .

**Assumption 5.3.** The norms of the velocity field  $v_k$  is A-Lipschitz, then for any  $z \in \mathbb{R}^d$ ,  $\|v_k(z)\| \leq A\|z\| + \|v_k(0)\| := A\|z\| + B$ .

This assumption of  $v_k$  corresponds to Cheng et al. [2023].

**Assumption 5.4.** The absolute moments of  $\mu_t$  is bounded by  $m_\alpha$  for  $\alpha \leq 5$ . i.e.  $\int \|z\|^\alpha d\mu_t(z) \leq m_\alpha < \infty$ .

Now we present the descent lemma of Algorithm 1.

**Proposition 5.5.** Suppose Assumption 5.1, 5.2, 5.3, 5.4 hold. Then the following inequality holds for  $h < \frac{1}{A}$ :  $\mathcal{F}(\hat{\mu}_{(k+1)h}) - \mathcal{F}(\hat{\mu}_{kh}) \leq -\frac{1}{2}h\|\nabla_{W_2}\mathcal{F}(\mu_{kh})\|_{L^2(\mu_{kh})}^2 + \frac{1}{2}h\epsilon_k + h^2[Cm_3 + M] + h^3[Cm_5 + M]$ , where  $C, M$  are constants that do not relate to  $k$  or  $h$ .

Please refer to appendix B.1 for detailed proof. We generalize the results of Huix et al. [2024], from  $n$ -dirac distribution to general gaussian-based semi-implicit distributions. The dependencies in Proposition 5.5 does not include the number of modes  $n$  which can go to infinity.

Using the above descent lemma, we obtain the convergence of the average of squared gradient norms.

**Theorem 5.6.** Assume Proposition 5.5 holds, then the average of squared gradient norms satisfies  $\frac{1}{K} \sum_{k=1}^K \|\nabla_{W_2}\mathcal{F}(\mu_{kh})\|_{L^2(\mu_{kh})}^2 \leq \frac{R}{K^{\frac{1}{2}}} + \frac{S}{K^{\frac{2}{3}}} + \frac{1}{K} \sum_{k=1}^K \epsilon_k$  for  $K > \min\{\frac{A^2\mathcal{F}(\hat{\mu}_0)}{Cm_3 + M}, \frac{A^3\mathcal{F}(\hat{\mu}_0)}{Cm_5 + M}\}$ , where  $R := 4\sqrt{\mathcal{F}(\hat{\mu}_0)(Cm_3 + M)}$  and  $S := 4(\mathcal{F}(\hat{\mu}_0))^{\frac{2}{3}}(Cm_5 + M)^{\frac{1}{3}}$ .

Please refer to appendix B.1 for detailed proof. Taking  $K \rightarrow \infty$  implies that the average of squared gradient norms is at the order of the average training error.

## 5.2 Statistical Guarantees

In this section, we further focus on the sample complexity required to satisfy Assumption 5.1. Specifically, we establish a statistical guarantee of the score matching for certain neural network family via empirical risk minimization (ERM).

We formally define the deep ReLU neural network family as  $\mathcal{S}(L, W, M, S, B) := \{s(x) = (A_L \sigma(\cdot) + b_L) \circ \dots \circ (A_1 x + b_1) : A_i \in \mathbb{R}^{d_i \times d_{i+1}}, b_i \in \mathbb{R}^{d_{i+1}}, \max d_i \leq W, \sum_{i=1}^L (\|A_i\|_0 + \|b_i\|_0) \leq S, \max \|A_i\|_\infty \vee \|b_i\|_\infty \leq B, \sup_x \|s(x)\|_\infty \leq M\}$ , where  $\sigma(x) = \max\{x, 0\}$ .

Consider ERM  $\hat{f}_\gamma := \arg \min_{f_\gamma \in \mathcal{S}} \frac{1}{n} \sum_{i=1}^n \ell(z_i; f_\gamma)$ , where  $\ell(z; f_\gamma) := \mathbb{E}_{q_\sigma(x|z)} \|f_\gamma(x) - \nabla \log q_\sigma(x|z)\|^2$  and  $\{z_i\}$  are i.i.d. samples of  $\mu(z)$ . The population loss is given by  $\ell(f_\gamma) := \mathbb{E}_{\mu(z)q_\sigma(x|z)} \|f_\gamma(x) - \nabla \log q_\sigma(x|z)\|^2 = \mathbb{E}_{\hat{\mu}(x)} \|f_\gamma(x) - \nabla \log \hat{\mu}(x)\|^2 + c_* =: \ell_{sm}(f_\gamma) + c_*$ , where  $c_* = \mathbb{E}_{\mu(z)q(x|z)} \|\nabla \log \hat{\mu}(x) - \nabla \log q(x|z)\|^2$  is a constant independent of  $f_\gamma$ .

**Assumption 5.7.**  $\mu(z)$  is sub-Gaussian, i.e., there exists  $C_1, C_2 > 0$  such that  $\mu(x) \leq C_1 \exp(-C_2 \|z\|^2)$ .

**Theorem 5.8.** *Under Assumption 5.7, for any  $\delta > 0$ , it holds with probability no less than  $1 - 2\delta$  that,*

$$\ell_{sm}(\hat{f}_\gamma) \leq 2 \inf_{f_\gamma \in \mathcal{S}} \ell_{sm}(f_\gamma) + \mathcal{O} \left( \sqrt{\frac{c_*(M^2 + \frac{d}{\sigma^2})}{n} \log \frac{\mathcal{N}}{\delta}} \right). \quad (5.4)$$

where  $\log \mathcal{N} = SL \log(WLB\sigma \log(\frac{dn}{\delta}))$ .

Please refer to appendix B.2 for detailed proof. This theorem suggest that when the approximation error of neural network family is negligible, we can get a  $\tilde{\mathcal{O}}(\frac{1}{\sqrt{n}})$ -accurate score estimation with high probability, where  $n$  is the particle number. Together with Theorem 5.6, we conclude that the total sample complexity to achieve  $\varepsilon$ -accuracy is  $K \cdot n = \tilde{\mathcal{O}}(1/\varepsilon^4)$ , exhibiting the sample efficiency of our methods.

## 6 Numerical Experiments

In this section, we compare SIFG and Ada-SIFG with other ParVI methods including SVGD [Liu and Wang, 2016],  $L_2$ -GF [di Langosco et al., 2021] and Ada-GWG [Cheng et al., 2023] on both synthetic and real data problems. In BNN experiments, we also test SGLD [Welling and Teh, 2011]. Through out this section, the initial particle distribution is the standard gaussian distribution except for the gaussian mixture experiments. For Ada-SIFG, the noise magnitude  $\sigma$  is clipped to be

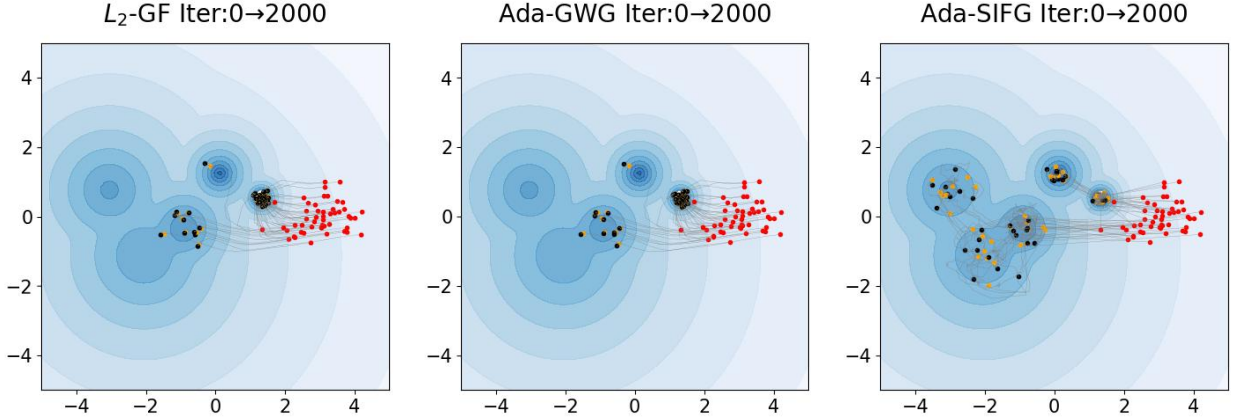


Figure 2: The moving trajectory of particles from initial to 2000 iterations of different methods. The red dot is the initial location, the orange dot is the particle location at 1600 iteration and the black dot is the location at 2000 iteration. We randomly choose 50 particles for illustration.

larger than 0.001 unless otherwise specified. Please refer to appendix C for more detailed setting information.

## 6.1 Gaussian Mixture

Utilizing the semi-implicit type of variational family incorporate the advantages of better exploration ability and the sample diversity. To visualize the effectiveness of our method, our first example is sampling from a 2D toy Gaussian mixture distribution. We compare with ParVI methods  $L_2$ -GF [di Langosco et al., 2021] and Ada-GWG [Cheng et al., 2023] on a 5-mode gaussian mixture distribution which the marginal probability of each cluster is  $1/5$ , and the standard deviations are 0.1, 0.2, 0.3, 0.4, 0.5. The initial distribution is the gaussian distribution  $\mathcal{N}((3, 0), 0.25\mathbf{I})$ . From figure 1 we can see that the samples of  $L_2$ -GF and Ada-GWG both stuck at certain modes at convergence, while SIFG uniformly covers all the modes because of incorporating better exploration ability. To illustrate the exploration ability and the sample diversity of SIFG compared to other methods, we randomly choose 50 particles of each methods and trace the moving trajectories of these particles from iteration 0 to 2000. We also denote the particles in orange at iteration 1600 where all methods converge in distribution. From figure 2 we can see that the particles of  $L_2$ -GF and Ada-GWG barely move near convergence (from iteration 1600 to 2000), while the particles of SIFG vary due to perturbation at each training epoch but still preserve the sampling quality.

To further quantitatively compare with other methods, we consider the 5-cluster 10D Gaussian

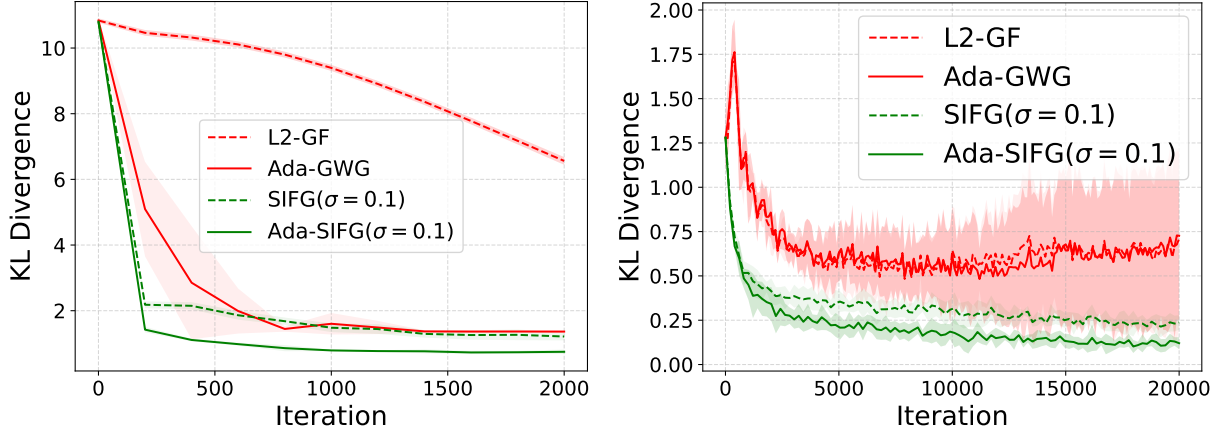


Figure 3: **Left:** KL divergence of different methods versus number of iterations on gaussian mixture distribution. **Right:** KL divergence of different methods versus number of iterations on the monomial gamma distribution.

mixture where the variances of the mixture components are 0.1, 0.2, 0.3, 0.4 and 0.5. The number of particles is 1000. The initial noise magnitude for both SIFG and Ada-SIFG is 0.1. The left of figure 3 shows the KL divergence against different numbers of iterations. On this toy example, SIFG with fixed noise level 0.1 significantly accelerates the convergence compared to  $L_2$ -GF, while being competitive against Ada-GWG. Ada-SIFG continues to improve the convergence of SIFG. This result demonstrates the effectiveness of injecting noise into the sampling process.

## 6.2 Monomial Gamma

To further investigate the exploration advantage of SIFG, following Cheng et al. [2023], we consider the heavy tailed 2D Monomial Gamma distribution where the target  $\pi(x_1, x_2) \propto \exp(-0.3(|x_1|^{0.9} + |x_2|^{0.9}))$ . The number of particles is 1000. The initial noise magnitude for both SIFG and Ada-SIFG is 0.1. Similar to the gaussian mixture experiment, the right of figure 3 shows SIFG converges faster than  $L_2$ -GF and Ada-GWG, and Ada-SIFG converges even faster than SIFG. Both SIFG and Ada-SIFG converge more steadily than  $L_2$ -GF and Ada-GWG. Additionally, the variances of SIFG and Ada-SIFG are also significantly smaller than which of  $L_2$ -GF and Ada-GWG. Faster convergence indicates higher exploration ability to efficiently traverse the heavy tail. This is achieved by perturbing the particles during training. Being able to use denoising score matching to estimate the score function contributes to the smaller variance.

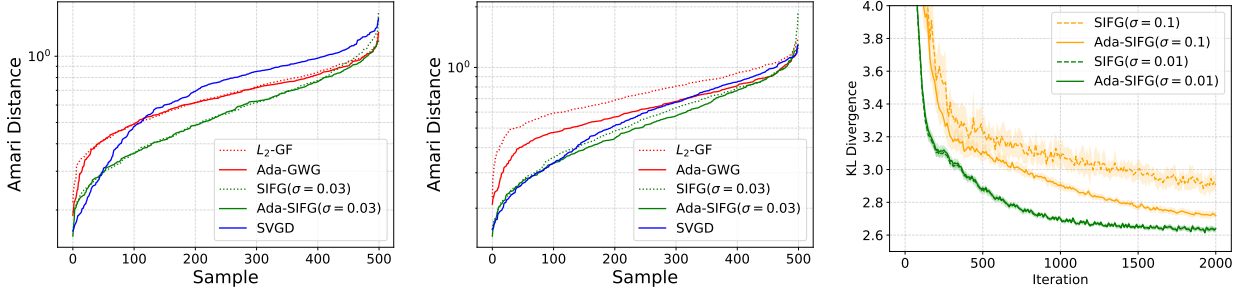


Figure 4: **Left and Middle:** Sorted Amari distances of different methods on MEG dataset. On the left is the experiment for 10 particles and 50 random repetitions. In the middle is the experiment for 100 particles and 5 random repetitions. **Right:** Test RMSE for BNN on Boston dataset. The number in parentheses specifies the initial  $\sigma$ . The results are averaged from 10 independent runs.

### 6.3 Independent Component Analysis

The task of Bayesian independent component analysis (ICA) is to infer the unknown unmixing matrix  $W \in \mathbb{R}^{d \times d}$  given the observations  $x$  from  $x = W^{-1}s$ , where  $s \in \mathbb{R}^d$  are the latent independent sources. Suppose  $X = \{x_n \in \mathbb{R}^d\}$  are the observed samples, assuming each component  $s_i$  has the same distribution  $s_i \sim p_s$ , then the likelihood is:

$$p(x|W) = |\det W| \prod_{i=1}^d p_s([Wx]_i)$$

Following [Korba et al. \[2021\]](#), we choose a gaussian prior over the unmixing matrix  $p(W_{ij}) \sim \mathcal{N}(0, \theta^2)$  and choose  $p_s(\cdot) = (\cosh(\cdot))^{-1}$ . We compare our methods SIFG and Ada-SIFG with KSDD, SVGD, L2GF and Ada-GWG on the MEG dataset [[Vigario et al., 1997](#)], which has 122 channels and 17730 observations. We extract the first 5 channels such that  $d = 5$  and the dimension of matrix  $W$  is 25. We compute the Amari distance [[Amari et al., 1995](#)] between the ground truth  $W_0$  estimated by using a long run ( $10^5$  samples) of standard HMC algorithm and the estimates generated by different methods to assess convergence. The measure equals to zero if and only if the two matrices are the same up to scale and permutation.

To assess the sample efficiency of different methods, we choose 10 and 100 particles for sampling, and we independently repeat 50 and 5 times so that we collect 500 samples for each method. The left and middle of figure 4 shows the Amari distance results after sorting. SIFG outperforms  $L_2$ -GF and Ada-GWG in both particle number settings, and is not significantly affected by the relatively small number of particles. On the contrary, SVGD is apparently affected by small particle size.

The improvement for both adaptive methods Ada-GWG and Ada-SIFG is not significant for small number of particles, while evident for larger number of particles. This is because the number of particles affects the training of neural networks. This suggests that the effectiveness of the adaptation procedure relies on the approximation accuracy of neural networks.

## 6.4 Bayesian Neural Networks

We compare our algorithm with SGLD, SVGD,  $L_2$ -GF and Ada-GWG on Bayesian neural networks (BNN). Following [Cheng et al., 2023], we conduct the two-layer network with 50 hidden units and ReLU activation function, and we use a Gamma(1, 0.1) prior for the inverse covariances. The datasets are all randomly partitioned into 90% for training and 10% for testing. The mini-batch size is 100 for all datasets. All results are averaged over 10 independent random trials. Table 1 shows the average test RMSE and NLL with their standard deviation. We see that Ada-SIFG can achieve comparable or better results than the other methods. Ada-SIFG consistently improves over  $L_2$ -GF by a noticeable margin. To examine the effect of adaptively tuning the noise magnitude  $\sigma$ , we additionally compare the test RMSE against iterations for two sets of SIFG and Ada-SIFG with different  $\sigma$  initialization. From the right of figure 4 we can see that on this specific task, setting  $\sigma = 0.01$  produces better results than  $\sigma = 0.1$ . Although the latter is sub-optimal, our adaptive method makes significant improvements, approaching toward the better performance of initializing  $\sigma = 0.01$ . The adaptive scheme serves as a correction on selecting proper  $\sigma$  automatically during training. This suggests that our adaptive method is robust even when the initial noise magnitude choice is not ideal. More experiment setting details can be found in the appendix C.

Table 1: Test RMSE and test NLL of Bayesian neural networks on several UCI datasets. The results are averaged from 10 independent runs with the standard deviation in the subscripts.

Dataset	Test RMSE ( $\downarrow$ )					Test NLL ( $\downarrow$ )				
	SGLD	SVGD	$L_2$ -GF	Ada-GWG	Ada-SIFG	SGLD	SVGD	$L_2$ -GF	Ada-GWG	Ada-SIFG
BOSTON	2.917 $\pm$ 0.04	2.944 $\pm$ 0.03	3.016 $\pm$ 0.12	2.662 $\pm$ 0.06	<b>2.641</b> $\pm$ 0.02	2.563 $\pm$ 0.01	2.567 $\pm$ 0.01	2.706 $\pm$ 0.04	2.680 $\pm$ 0.04	<b>2.496</b> $\pm$ 0.02
CONCRETE	8.218 $\pm$ 0.27	7.640 $\pm$ 0.03	7.556 $\pm$ 0.08	<b>6.590</b> $\pm$ 0.09	6.619 $\pm$ 0.03	3.539 $\pm$ 0.02	3.455 $\pm$ 0.01	3.449 $\pm$ 0.01	3.341 $\pm$ 0.01	<b>3.323</b> $\pm$ 0.01
POWER	4.176 $\pm$ 0.01	4.940 $\pm$ 0.00	4.258 $\pm$ 0.06	4.074 $\pm$ 0.05	<b>4.017</b> $\pm$ 0.00	2.863 $\pm$ 0.00	3.016 $\pm$ 0.00	3.070 $\pm$ 0.02	2.967 $\pm$ 0.01	<b>2.829</b> $\pm$ 0.00
WINE	0.431 $\pm$ 0.00	0.422 $\pm$ 0.00	0.419 $\pm$ 0.00	0.416 $\pm$ 0.00	<b>0.413</b> $\pm$ 0.00	0.576 $\pm$ 0.00	0.559 $\pm$ 0.00	0.552 $\pm$ 0.01	0.552 $\pm$ 0.00	<b>0.535</b> $\pm$ 0.00
PROTEIN	<b>4.609</b> $\pm$ 0.00	4.940 $\pm$ 0.00	5.024 $\pm$ 0.02	4.967 $\pm$ 0.01	4.863 $\pm$ 0.00	<b>2.946</b> $\pm$ 0.00	3.016 $\pm$ 0.00	3.075 $\pm$ 0.02	3.040 $\pm$ 0.01	2.999 $\pm$ 0.00
DIABETES	0.382 $\pm$ 0.00	0.386 $\pm$ 0.00	0.381 $\pm$ 0.00	0.384 $\pm$ 0.00	<b>0.379</b> $\pm$ 0.00	0.466 $\pm$ 0.00	0.484 $\pm$ 0.00	0.471 $\pm$ 0.00	0.479 $\pm$ 0.00	<b>0.449</b> $\pm$ 0.00

## 7 Conclusion

We presented a new functional gradient flow method, called SIFG, which utilizes the semi-implicit variational family represented by particles by injecting gaussian noise to the particles before updating according to the gradient flow. We generalize the convergence guarantees of variational inference with gaussian mixtures in discrete time setting. We considered the sample complexity in the ERM regime. We also introduced an adaptive version, called Ada-SIFG, that can automatically tune the noise magnitude to improve sampling quality. Extensive numerical experiments showed that Ada-SIFG outperforms existing ParVI methods.

## Acknowledgements

This work was supported by National Natural Science Foundation of China (grant no. 12201014 and grant no. 12292983). The research of Cheng Zhang was supported in part by National Engineering Laboratory for Big Data Analysis and Applications, the Key Laboratory of Mathematics and Its Applications (LMAM) and the Key Laboratory of Mathematical Economics and Quantitative Finance (LMEQF) of Peking University. The authors are grateful for the computational resources provided by the High-performance Computing Platform of Peking University.

## References

- David Alvarez-Melis, Yair Schiff, and Youssef Mroueh. Optimizing functionals on the space of probabilities with input convex neural networks. *Transactions on Machine Learning Research*, 2022. ISSN 2835-8856. URL <https://openreview.net/forum?id=dp0YN7o8Jm>.
- S. I. Amari, A. Cichocki, and H. Yang. A new learning algorithm for blind signal separation. *Advances in neural information processing systems*, 8, 1995.
- David M. Blei, Alp Kucukelbir, and Jon D. McAuliffe. Variational inference: A review for statisticians. *Journal of the American Statistical Association*, 112:859 – 877, 2016.
- Olivier Bousquet. *Concentration inequalities and empirical processes theory applied to the analysis of learning algorithms*. PhD thesis, École Polytechnique: Department of Applied Mathematics Paris, France, 2002.

- Changyou Chen, Ruiyi Zhang, Wenlin Wang, Bai Li, and Liqun Chen. A unified particle-optimization framework for scalable bayesian sampling. *ArXiv*, abs/1805.11659, 2018.
- Tianqi Chen, Emily Fox, and Carlos Guestrin. Stochastic gradient hamiltonian monte carlo. In *International Conference on Machine Learning*, pages 1683–1691, 2014.
- Z. Cheng, S. Zhang, L. Yu, and C. Zhang. Particle-based variational inference with generalized wasserstein gradient flow. *Advances in Neural Information Processing Systems*, 2023.
- Ziheng Cheng, Longlin Yu, Tianyu Xie, Shiyue Zhang, and Cheng Zhang. Kernel semi-implicit variational inference. *arXiv preprint arXiv:2405.18997*, 2024.
- Sinho Chewi, Thibaut Le Gouic, Chen Lu, Tyler Maunu, and Philippe Rigollet. Svgd as a kernelized wasserstein gradient flow of the chi-squared divergence. *Advances in Neural Information Processing Systems*, 33, 2020.
- Lauro Langosco di Langosco, Vincent Fortuin, and Heiko Strathmann. Neural variational gradient descent. *arXiv preprint arXiv:2107.10731*, 2021.
- Michael Diao, Krishnakumar Balasubramanian, Sinho Chewi, and Adil Salim. Forward-backward gaussian variational inference via jko in the bures–wasserstein space. In *International Conference on Machine Learning*, pages 7960–7991, 2023.
- Hanze Dong, Xi Wang, LIN Yong, and Tong Zhang. Particle-based variational inference with preconditioned functional gradient flow. In *The Eleventh International Conference on Learning Representations*, 2023. URL <https://openreview.net/forum?id=60phWWAE3cS>.
- S. Duane, A. D. Kennedy, B J. Pendleton, and D. Roweth. Hybrid Monte Carlo. *Physics Letters B*, 195(2):216 – 222, 1987.
- Jiaojiao Fan, Qinsheng Zhang, Amirhossein Taghvaei, and Yongxin Chen. Variational wasserstein gradient flow. In *International Conference on Machine Learning*, pages 6185–6215. PMLR, 2022.
- Will Grathwohl, Kuan-Chieh Wang, Jörn-Henrik Jacobsen, David Duvenaud, and Richard Zemel. Learning the stein discrepancy for training and evaluating energy-based models without sampling. In *International Conference on Machine Learning*, pages 3732–3747. PMLR, 2020.
- Tianyang Hu, Zixiang Chen, Hanxi Sun, Jincheng Bai, Mao Ye, and Guang Cheng. Stein neural sampler. *arXiv preprint arXiv:1810.03545*, 2018.



- Tom Huix, Anna Korba, Alain Durmus, and Eric Moulines. Theoretical guarantees for variational inference with fixed-variance mixture of gaussians. *arXiv preprint arXiv:2406.04012*, 2024.
- Michael I. Jordan, Zoubin Ghahramani, T. Jaakkola, and Lawrence K. Saul. An introduction to variational methods for graphical models. *Machine Learning*, 37:183–233, 1999.
- Anna Korba, Pierre-Cyril Aubin-Frankowski, Szymon Majewski, and Pierre Ablin. Kernel stein discrepancy descent. In *International Conference on Machine Learning*, pages 5719–5730. PMLR, 2021.
- Marc Lambert, Sinho Chewi, Francis Bach, Silvere Bonnabel, and Philippe Rigollet. Variational inference via wasserstein gradient flows. *Advances in Neural Information Processing Systems*, 35, 2022.
- Jen Ning Lim and Adam Johansen. Particle semi-implicit variational inference. *arXiv preprint arXiv:2407.00649*, 2024.
- Chang Liu, Jingwei Zhuo, Pengyu Cheng, Ruiyi Zhang, Jun Zhu, and Lawrence Carin. Understanding and accelerating particle-based variational inference. *International Conference on Machine Learning*. PMLR, pp. 4082-4092, 2019.
- Qiang Liu. Stein variational gradient descent as gradient flow. *Advances in neural information processing systems*, 30, 2017.
- Qiang Liu and Dilin Wang. Stein variational gradient descent: A general purpose bayesian inference algorithm. *Advances in neural information processing systems*, 29, 2016.
- Weijian Luo, Tianyang Hu, Shifeng Zhang, Jiacheng Sun, Zhenguo Li, and Zhihua Zhang. Diff-instruct: A universal approach for transferring knowledge from pre-trained diffusion models. *Advances in Neural Information Processing Systems*, 36, 2024.
- Radford Neal. MCMC using hamiltonian dynamics. In S Brooks, A Gelman, G Jones, and XL Meng, editors, *Handbook of Markov Chain Monte Carlo*, Chapman & Hall/CRC Handbooks of Modern Statistical Methods. Taylor & Francis, 2011. ISBN 9781420079425. URL <http://books.google.com/books?id=qfRsAIKZ4rIC>.
- G. O. Robert and O. Stramer. Langevin diffusions and metropolis-hastings algorithms. *Methodology and Computing in Applied Probability*, 4:337–357, 2002.

- Nathan Srebro, Karthik Sridharan, and Ambuj Tewari. Smoothness, low noise and fast rates. *Advances in neural information processing systems*, 23, 2010.
- Michalis K Titsias and Francisco Ruiz. Unbiased implicit variational inference. In *The 22nd International Conference on Artificial Intelligence and Statistics*, pages 167–176. PMLR, 2019.
- R. Vigario, J. Sarela, and E. Oja. Meg data for studies using independent component analysis. 1997. URL <http://www.cis.hut.fi/projects/ica/eegmeg/MEGdata.html>.
- Pascal Vincent. A connection between score matching and denoising autoencoders. *Neural computation*, 23(7):1661–1674, 2011.
- M. J. Wainwright and M. I. Jordan. Graphical models, exponential families, and variational inference. *Foundations and Trends in Machine Learning*, 1(1-2):1–305, 2008.
- Martin J Wainwright. *High-dimensional statistics: A non-asymptotic viewpoint*, volume 48. Cambridge university press, 2019.
- Max Welling and Yee W Teh. Bayesian learning via stochastic gradient langevin dynamics. In *International Conference on Machine Learning*, pages 681–688, 2011.
- Mingzhang Yin and Mingyuan Zhou. Semi-implicit variational inference. In *International Conference on Machine Learning*, pages 5660–5669. PMLR, 2018.
- Longlin Yu and Cheng Zhang. Semi-implicit variational inference via score matching. *arXiv preprint arXiv:2308.10014*, 2023.

## A Details of Ada-SIFG

We follow the derivation idea of Luo et al. [2024] to prove the gradient estimate result (4.22).

$$\frac{d}{d\sigma} \mathcal{F}_\sigma(\mu_t) = \mathbb{E}_{z \sim \mu_t(z), w \sim \mathcal{N}(0, I)} \frac{\partial}{\partial \sigma} \log \frac{\hat{\mu}_{\sigma, t}(z + \sigma w)}{\pi(z + \sigma w)} \quad (\text{A.1})$$

$$= \mathbb{E}_{z \sim \mu_t(z), w \sim \mathcal{N}(0, I)} \nabla \log \frac{\hat{\mu}_{\sigma, t}(z + \sigma w)}{\pi(z + \sigma w)} \cdot w + \mathbb{E}_{x \sim \hat{\mu}_{\sigma, t}} \frac{\partial}{\partial \sigma} \log \hat{\mu}_{\sigma, t}(x) \quad (\text{A.2})$$

$$= \mathbb{E}_{z \sim \mu_t(z), w \sim \mathcal{N}(0, I)} \nabla \log \frac{\hat{\mu}_{\sigma, t}(z + \sigma w)}{\pi(z + \sigma w)} \cdot w \quad (\text{A.3})$$

$$\approx \mathbb{E}_{z \sim \mu_t(z), w \sim \mathcal{N}(0, I)} [f_\gamma(z + \sigma w) - \nabla \log \pi(z + \sigma w)] \cdot w \quad (\text{A.4})$$

where the equality of (A.4) is because

$$\mathbb{E}_{x \sim \hat{\mu}_{\sigma, t}} \frac{\partial}{\partial \sigma} \log \hat{\mu}_{\sigma, t}(x) = \int \frac{\partial}{\partial \sigma} \hat{\mu}_{\sigma, t}(x) dx = \frac{\partial}{\partial \sigma} \int \hat{\mu}_{\sigma, t}(x) dx = \frac{\partial}{\partial \sigma} 1 = 0. \quad (\text{A.5})$$

By this gradient descent scheme on the noise magnitude  $\sigma$ , we present the full procedure of Ada-SIFG in Algorithm 2.

## B Proofs

### B.1 Proof of Proposition 5.5 and Theorem 5.6

#### B.1.1 Main Lemmas

**Lemma B.1.** *Assuming the second moment of distribution  $\rho$  is finite,  $k_\sigma(x) = Z_0 e^{-\frac{\|x\|^2}{2\sigma^2}}$ , where  $Z_0$  satisfies  $\int k_\sigma(x) dx = 1$ , then for all  $\theta \in \mathbb{R}^d$ ,  $k \in \mathbb{N}_+$ , there exists constant  $C, M > 0$ , such that*

$$\frac{\int \|\theta - y\|^k k_\sigma(\theta - y) d\rho(y)}{\int k_\sigma(\theta - y) d\rho(y)} \leq C \|\theta\|^k + M \quad (\text{B.1})$$

*Proof.* Since  $\int y^2 d\rho(y) < \infty$ , there exists a sufficient large constant  $R_0$  and a positive constant  $C_0 > 0$ , both do not relate to  $\theta$ , such that  $\int_{\|y\| < R} y^2 d\rho(y) > C_0$  for all  $R \geq R_0$ , then  $\int_{\|y\| < R} d\rho(y) > \frac{C_0}{R_0^2}$  for all  $R \geq R_0$ . Note that  $\{y : \|\theta - y\| < R_0 + \|\theta\|\} \supseteq \{y : \|y\| < R_0\}$  by triangular inequality, we have  $\int_{\|\theta - y\| < R_0 + \|\theta\|} y^2 d\rho(y) > C_0$ .

---

**Algorithm 2** Ada-SIFG: adaptive semi-implicit functional gradient flow
 

---

**Require:** Unnormalized target distribution  $\pi$ , initial particles  $\{z_0^i\}_{i=1}^n$ , initial parameter  $\gamma_0$ , iteration number  $N, N'$ , particle step size  $h$ , parameter step size  $\eta$ , initial noise magnitude  $\sigma_0$ , noise magnitude step size  $\tilde{\eta}$ , lower and upper bounds on  $\sigma$ :  $lb, ub$ .

**for**  $k = 0, \dots, N - 1$  **do**

Assign  $\gamma_k^0 = \gamma_k$

Obtain perturbed samples  $x_k^i = z_k^i + \epsilon_k^i$ , where  $\epsilon_k^i \sim \mathcal{N}(0, \sigma_k^2)$

**for**  $t = 0, \dots, N' - 1$  **do**

Compute

$$\widehat{\mathcal{L}}(\gamma) = \frac{1}{n} \sum_{i=1}^n \left\| f_\gamma(x_k^i) - \frac{x_k^i - z_k^i}{\sigma_k^2} \right\|^2 \quad (\text{A.6})$$

Update  $\gamma_k^{t+1} = \gamma_k^t + \eta \nabla_\gamma \widehat{\mathcal{L}}(\gamma_k^t)$

**end for**

Update  $\gamma_{k+1} = \gamma_k^{N'}$

Compute  $\widehat{\text{grad}}(\sigma_k) = \frac{1}{n} \sum_{i=1}^n [\nabla \log \pi(x_k^i) - f_{\gamma_{k+1}}(x_k^i)] \cdot \epsilon_k^i$

Update  $\sigma_{k+1} = \text{clip}(\sigma_k + \tilde{\eta} \cdot \widehat{\text{grad}}(\sigma_k), lb, ub)$

Update particles  $z_{k+1}^i = z_k^i + h(\nabla \log \pi(x_k^i) - f_{\gamma_{k+1}}(x_k^i))$  for  $i = 1, \dots, n$

**end for**

Obtain perturbed samples  $x_N^i = z_N^i + \epsilon_N^i$ , where  $\epsilon_N^i \sim \mathcal{N}(0, \sigma_N^2)$

**return** Particles  $\{x_N^i\}_{i=1}^n$

---

From the above analysis, the denominator

$$\begin{aligned} \int k_\sigma(\theta - y) d\rho(y) &> \int_{\|\theta - y\| < R_0 + \|\theta\|} k_\sigma(\theta - y) d\rho_t(y) \\ &> \int_{\|\theta - y\| < R_0 + \|\theta\|} e^{-\frac{(R_0 + \|\theta\|)^2}{2\sigma^2}} d\rho(y) \\ &> Z_0 \int_{\|y\| < R_0} e^{-\frac{(R_0 + \|\theta\|)^2}{2\sigma^2}} d\rho(y) \\ &> Z_0 e^{-\frac{(R_0 + \|\theta\|)^2}{2\sigma^2}} \cdot \frac{C_0}{R_0^2} \end{aligned} \quad (\text{B.2})$$

Then

$$\frac{\int \|\theta - y\|^k k_\sigma(\theta - y) d\rho(y)}{\int k_\sigma(\theta - y) d\rho(y)} = \frac{\int_{\|\theta - y\| > R} \|\theta - y\|^k k_\sigma(\theta - y) d\rho(y) + \int_{\|\theta - y\| < R} \|\theta - y\|^k k_\sigma(\theta - y) d\rho(y)}{\int k_\sigma(\theta - y) d\rho(y)} \quad (\text{B.3})$$

$$\leq \frac{\int_{\|\theta - y\| > R} \|\theta - y\|^k k_\sigma(\theta - y) d\rho(y)}{\int k_\sigma(\theta - y) d\rho(y)} + R^k \quad (\text{B.4})$$

$$\leq \frac{Z_0 R^k e^{-\frac{R^2}{2\sigma^2}}}{\int k_\sigma(\theta - y) d\rho(y)} + R^k \quad (\text{B.5})$$

$$\leq \frac{R^k e^{-\frac{R^2}{2\sigma^2}}}{e^{-\frac{(R_0 + \|\theta\|)^2}{2\sigma^2}}} \cdot \frac{R_0^2}{C_0} + R^k \quad (\text{B.6})$$

The inequality (B.5) uses monotonically decreasing property for  $R^k e^{-\frac{R^2}{2\sigma^2}}$  when  $R > R_1 = \sqrt{k}\sigma$ , and plugging in (B.2) gives the inequality (B.6).

Choose  $R = \max\{R_0 + \|\theta\|, R_1\}$ , we have  $\frac{\int \|\theta - y\|^k k_\sigma(\theta - y) d\rho(y)}{\int k_\sigma(\theta - y) d\rho(y)} \leq (\frac{R_0^2}{C_0} + 1)R^k \leq C(\|\theta\|^k + M)$ , where  $C = (\frac{R_0^2}{C_0} + 1)2^{k-1}$ ,  $M = (\frac{R_0^2}{C_0} + 1) \cdot \max\{2^{k-1}R_0^k, R_1^k\}$ , the proof is complete.  $\square$

**Lemma B.2.** Denote  $\psi_t = Id + t\phi$ , then for any  $\rho_0 \in \mathcal{P}(\mathbb{R}^d)$  and  $\rho_t = (\psi_t)_\# \rho_0$ , we have

$$\left. \frac{d}{dt} \mathcal{G}(\hat{\rho}_t) - \frac{d}{dt} \mathcal{G}(\hat{\rho}_t) \right|_{t=0} \leq Lt \|\phi\|_{L^2(\rho_0)}^2 \quad (\text{B.7})$$

where  $\mathcal{G}(\hat{\rho}_t) := \int -\log \pi(x) d\hat{\mu}_t(x)$ ,  $L$  is the Lipschitz constant of  $\nabla \log \pi$ .

*Proof.* Analogous to (4.14),

$$\frac{d}{dt} \mathcal{G}(\hat{\rho}_t) = \left\langle \int -\nabla \log \pi(x) q_\sigma(x|z) dx, \phi(\psi_t^{-1}(z)) \right\rangle_{L^2(\rho_t)} \quad (\text{B.8})$$

Then

$$\begin{aligned} \left. \frac{d}{dt} \mathcal{G}(\hat{\rho}_t) - \frac{d}{dt} \mathcal{G}(\hat{\rho}_t) \right|_{t=0} &= \left\langle \int -\nabla \log \pi(x) q_\sigma(x|z) dx, \phi(\psi_t^{-1}(z)) \right\rangle_{L^2(\rho_t)} - \left\langle \int -\nabla \log \pi(x) q_\sigma(x|z) dx, \phi(z) \right\rangle_{L^2(\rho_0)} \\ &= \left\langle \left[ \int -\nabla \log \pi(x) q_\sigma(x|\psi_t(z)) dx - \int -\nabla \log \pi(x) q_\sigma(x|z) dx \right], \phi(z) \right\rangle_{L^2(\rho_0)} \\ &= \left\langle \int [\nabla \log \pi(x) - \nabla \log \pi(x + t\phi(z))] q_\sigma(x|z) dx, \phi(z) \right\rangle_{L^2(\rho_0)} \\ &\leq \langle L \|t\phi(z)\|, \|\phi(z)\| \rangle_{L^2(\rho_0)} = Lt \|\phi\|_{L^2(\rho_0)}^2 \end{aligned} \quad (\text{B.9})$$

□

**Lemma B.3.** Denote  $\psi_t = Id + t\phi$ , where  $\|\phi(z)\| \leq A\|z\| + B$ , then for any fifth absolute moment finite  $\rho_0 \in \mathcal{P}(\mathbb{R}^d)$  and  $\rho_t = (\psi_t)_\# \rho_0$ ,  $t < \frac{1}{A}$ , there exists constants  $C, M$  such that

$$\left. \frac{d}{dt} \mathcal{E}(\hat{\rho}_t) - \frac{d}{dt} \mathcal{E}(\hat{\rho}_t) \right|_{t=0} \leq t[Cm_3(\rho_0) + M] + t^2[Cm_5(\rho_0) + M] \quad (\text{B.10})$$

where  $\mathcal{E}(\hat{\mu}_t) := \int \log \hat{\mu}_t(x) d\hat{\mu}_t(x)$ ,  $m_3(\rho_0) := \int \|z\|^3 d\rho_0$  and  $m_5(\rho_0) := \int \|z\|^5 d\rho_0$  are the third and fifth absolute moments of  $\rho_0$ .

*Proof.* Analogous to (4.14),

$$\begin{aligned} \frac{d}{dt} \mathcal{E}(\hat{\rho}_t) &= \left\langle \int \nabla \log \hat{\rho}_t(x) q_\sigma(x|z) dx, \phi(\psi_t^{-1}(z)) \right\rangle_{L^2(\rho_t)} \\ &= \left\langle \int q_\sigma(x|z) \frac{\int \nabla_x q_\sigma(y|x) d\rho_t(y)}{\int q_\sigma(y|x) d\rho_t(y)} dx, \phi(\psi_t^{-1}(z)) \right\rangle_{L^2(\rho_t)} \end{aligned} \quad (\text{B.11})$$

Then

$$\begin{aligned} &\left. \frac{d}{dt} \mathcal{E}(\hat{\rho}_t) - \frac{d}{dt} \mathcal{E}(\hat{\rho}_t) \right|_{t=0} \\ &= \left\langle \int q_\sigma(x|z) \frac{\int \nabla_x q_\sigma(y|x) d\rho_t(y)}{\int q_\sigma(y|x) d\rho_t(y)} dx, \phi(\psi_t^{-1}(z)) \right\rangle_{L^2(\rho_t)} - \left\langle \int q_\sigma(x|z) \frac{\int \nabla_x q_\sigma(y|x) d\rho_0(y)}{\int q_\sigma(y|x) d\rho_0(y)} dx, \phi(z) \right\rangle_{L^2(\rho_0)} \\ &= \left\langle \left[ \int q_\sigma(x|\psi_t(z)) \frac{\int \nabla_x q_\sigma(y|x) d\rho_t(y)}{\int q_\sigma(y|x) d\rho_t(y)} dx - \int q_\sigma(x|z) \frac{\int \nabla_x q_\sigma(y|x) d\rho_0(y)}{\int q_\sigma(y|x) d\rho_0(y)} dx \right], \phi(z) \right\rangle_{L^2(\rho_0)} \\ &= \frac{1}{\sigma^2} \left\langle \left[ q_\sigma(x|\psi_t(z)) \frac{\int y q_\sigma(y|x) d\rho_t(y)}{\int q_\sigma(y|x) d\rho_t(y)} - q_\sigma(x|z) \frac{\int y q_\sigma(y|x) d\rho_0(y)}{\int q_\sigma(y|x) d\rho_0(y)} \right] dx, \phi(z) \right\rangle_{L^2(\rho_0)} + \frac{t}{\sigma^2} \|\phi\|_{L^2(\rho_0)}^2 \end{aligned} \quad (\text{B.12})$$

Denote  $A_t := q_\sigma(x|\psi_t(z)) \frac{\int y q_\sigma(y|x) d\rho_t(y)}{\int q_\sigma(y|x) d\rho_t(y)}$ , then  $A_0 = q_\sigma(x|z) \frac{\int y q_\sigma(y|x) d\rho_0(y)}{\int q_\sigma(y|x) d\rho_0(y)}$ .

For simplicity, we denote  $k_\sigma(w) = Z_0 e^{-\frac{\|w\|^2}{2\sigma^2}}$ , where  $Z_0$  satisfies  $\int k_\sigma(w) dw = 1$ , then  $q_\sigma(x|z) = k_\sigma(x - z)$ .

By Lagrangian mean value theorem, there exists  $t', t'' \in [0, t]$ , such that:

$$q_\sigma(x|\psi_t(z)) = Z_0 e^{-\frac{\|x - (z + t\phi(z))\|^2}{2\sigma^2}} = Z_0 \left[ e^{-\frac{\|x - z\|^2}{2\sigma^2}} + t \cdot e^{-\frac{\|x - (z + t'\phi(z))\|^2}{2\sigma^2}} \frac{(x - (z + t'\phi(z)))}{\sigma^2} \phi(z) \right] \quad (\text{B.13})$$

and

$$\frac{\int y k_\epsilon(x - y) d\rho_t(y)}{\int k_\sigma(x - y) d\rho_t(y)} = \frac{\int y k_\sigma(x - y) d\rho(y)}{\int k_\sigma(x - y) d\rho(y)} + t \cdot \left. \frac{\partial}{\partial t} \right|_{t=t''} \left( \frac{\int y k_\sigma(x - y) d\rho_t(y)}{\int k_\sigma(x - y) d\rho_t(y)} \right) \quad (\text{B.14})$$

Using continuity equation  $\frac{d\rho_t(y)}{dt} = -\nabla \cdot (\rho_t(y)\phi(\psi_t^{-1}(y)))$  for  $y \sim \rho_t$ , we have:

$$\frac{\partial \int y k_\sigma(x-y) d\rho_t(y)}{\partial t \int k_\sigma(x-y) d\rho_t(y)} \quad (\text{B.15})$$

$$= \frac{\int y k_\sigma(x-y) \frac{d\rho_t(y)}{dt} \int k_\sigma(x-y) d\rho_t(y) - \int y k_\sigma(x-y) d\rho_t(y) \int k_\sigma(x-y) \frac{d\rho_t(y)}{dt}}{(\int k_\sigma(x-y) d\rho_t(y))^2} \quad (\text{B.16})$$

$$= \frac{\int \phi(\psi_t^{-1}(y)) \nabla(y k_\sigma(x-y)) d\rho_t(y)}{\int k_\sigma(x-y) d\rho_t(y)} - \frac{\int y k_\sigma(x-y) d\rho_t(y) \int \phi(\psi_t^{-1}(y)) \nabla k_\sigma(x-y) d\rho_t(y)}{(\int k_\sigma(x-y) d\rho_t(y))^2} \quad (\text{B.17})$$

$$= \frac{\int \phi(\psi_t^{-1}(y)) (1 + y \frac{x-y}{\sigma^2}) k_\sigma(x-y) d\rho_t(y)}{\int k_\sigma(x-y) d\rho_t(y)} - \frac{\int y k_\sigma(x-y) d\rho_t(y) \int \phi(\psi_t^{-1}(y)) \frac{x-y}{\sigma^2} k_\sigma(x-y) d\rho_t(y)}{\int k_\sigma(x-y) d\rho_t(y)} \quad (\text{B.18})$$

Since  $\psi_t(y) = y + t\phi(y)$  and  $\|\phi(y)\| \leq A\|y\| + B$ , then  $(1-tA)\|y\| - tB \leq \|y\| - t\|\phi(y)\| \leq \|\psi_t(y)\|$ .

For  $t < \frac{1}{A}$ , we have  $\|y\| \leq \frac{1}{1-tA} \|\psi_t(y)\| + \frac{tB}{1-tA}$ , which means  $\|\psi_t^{-1}(y)\| \leq \frac{1}{1-tA} \|y\| + \frac{tB}{1-tA}$ .

This means that  $\|\phi(\psi_t^{-1}(y))\| \leq \frac{A}{1-tA} \|y\| + \frac{B}{1-tA}$ .

By triangular inequality, we have

$$\begin{aligned} & \|\phi(\psi_t^{-1}(y)) (1 + y \frac{x-y}{\sigma^2})\| \\ \leq & \frac{A}{(1-tA)\sigma^2} \|x-y\|^3 + (2\frac{A\|x\|}{(1-tA)\sigma^2} + \frac{B}{1-tA}) \|x-y\|^2 + (\frac{\|x\|}{\sigma^2} (\frac{A}{1-tA} \|x\| + \frac{B}{1-tA}) + \frac{A}{1-tA}) \|x-y\| \\ & + (\frac{A}{1-tA} \|x\| + \frac{B}{1-tA}) \end{aligned} \quad (\text{B.19})$$

The right hand side is a polynomial of  $(\|x\|, \|x-y\|)$ , the order of which is at most 3. Since the fifth moment of  $\rho_0$  is finite, then the second moment is also finite. Using basic inequalities  $\|x\|^3 + \frac{4}{27} \geq \|x\|^2$ ,  $\|x\|^3 + \frac{8}{27} \geq \|x\|$  and Lemma B.1, we obtain:

$$\left\| \frac{\int \phi(\psi_t^{-1}(y)) (1 + y \frac{x-y}{\sigma^2}) k_\sigma(x-y) d\rho_t(y)}{\int k_\sigma(x-y) d\rho_t(y)} \right\| \leq C_1 \|x\|^3 + M_1 \quad (\text{B.20})$$

where  $C_1, M_1 > 0$  are constants that does not relate to  $x$ .

Analogously,

$$\left\| \frac{\int y k_\sigma(x-y) d\rho_t(y) \int \phi(\psi_t^{-1}(y)) \frac{x-y}{\sigma^2} k_\sigma(x-y) d\rho_t(y)}{\int k_\sigma(x-y) d\rho_t(y)} \right\| \leq C_2 \|x\|^3 + M_2 \quad (\text{B.21})$$

To conclude, we obtain

$$\left\| \frac{\partial}{\partial t} \Big|_{t=t''} \left( \frac{\int y k_\sigma(x-y) d\rho_t(y)}{\int k_\sigma(x-y) d\rho_t(y)} \right) \right\| \leq (C_1 + C_2) \|x\|^3 + (M_1 + M_2) := C_3 \|x\|^3 + M_3 \quad (\text{B.22})$$

for  $t < \frac{1}{A}$ .

From (B.13) and (B.14) we have

$$\begin{aligned} & \frac{1}{Z_0} \|A_t - A_0\| \\ &= \left\| t \left[ \frac{\int y k_\sigma(x-y) d\rho(y)}{\int k_\sigma(x-y) d\rho(y)} \cdot e^{-\frac{\|x-(z+t'\phi(z))\|^2}{2\sigma^2}} \frac{(x-(z+t'\phi(z)))}{\sigma^2} \phi(z) + e^{-\frac{\|x-z\|^2}{2\sigma^2}} \cdot \frac{\partial}{\partial t} \Big|_{t=t''} \left( \frac{\int y k_\sigma(x-y) d\rho_t(y)}{\int k_\sigma(x-y) d\rho_t(y)} \right) \right] \right. \\ & \quad \left. + t^2 e^{-\frac{\|x-(z+t'\phi(z))\|^2}{2\sigma^2}} \frac{(x-(z+t'\phi(z)))}{\sigma^2} \phi(z) \cdot \frac{\partial}{\partial t} \Big|_{t=t''} \left( \frac{\int y k_\sigma(x-y) d\rho_t(y)}{\int k_\sigma(x-y) d\rho_t(y)} \right) \right\| \\ &\leq t \left[ \|\phi(z)\| (C_4 \|x\| + M_4) \left\| \frac{(x-(z+t'\phi(z)))}{\sigma^2} \right\| e^{-\frac{\|x-(z+t'\phi(z))\|^2}{2\sigma^2}} + e^{-\frac{\|x-z\|^2}{2\sigma^2}} \cdot (C_3 \|x\|^3 + M_3) \right] \\ & \quad + t^2 \|\phi(z)\| \left\| \frac{(x-(z+t'\phi(z)))}{\sigma^2} \right\| e^{-\frac{\|x-(z+t'\phi(z))\|^2}{2\sigma^2}} \cdot (C_3 \|x\|^3 + M_3) \end{aligned} \quad (\text{B.23})$$

Then

$$\begin{aligned} & \int \|q_\sigma(x|\psi_t(z)) \frac{\int y q_\sigma(y|x) d\rho_t(y)}{\int q_\sigma(y|x) d\rho_t(y)} - q_\sigma(x|z) \frac{\int y q_\sigma(y|x) d\rho_0(y)}{\int q_\sigma(y|x) d\rho_0(y)}\| dx \\ &= \int \|A_t - A_0\| dx \\ &\leq t Z_0 \int \left[ \|\phi(z)\| (C_4 \|x\| + M_4) \left\| \frac{(x-(z+t'\phi(z)))}{\sigma^2} \right\| e^{-\frac{\|x-(z+t'\phi(z))\|^2}{2\sigma^2}} + e^{-\frac{\|x-z\|^2}{2\sigma^2}} \cdot (C_3 \|x\|^3 + M_3) \right] dx \\ & \quad + t^2 Z_0 \int \|\phi(z)\| \left\| \frac{(x-(z+t'\phi(z)))}{\sigma^2} \right\| e^{-\frac{\|x-(z+t'\phi(z))\|^2}{2\sigma^2}} \cdot (C_3 \|x\|^3 + M_3) dx \\ &\leq t [(C_5 \|z + t'\phi(z)\| + M_5) \|\phi(z)\| + C_6 \|z\| + M_6] + t^2 (C_7 \|z + t'\phi(z)\|^3 + M_7) \|\phi(z)\| \end{aligned} \quad (\text{B.24})$$

Plugging in  $t' \leq t < \frac{1}{A}$  and  $\|\phi(z)\| \leq A\|z\| + B$ , we obtain

$$\int \|q_\sigma(x|\psi_t(z)) \frac{\int y q_\sigma(y|x) d\rho_t(y)}{\int q_\sigma(y|x) d\rho_t(y)} - q_\sigma(x|z) \frac{\int y q_\sigma(y|x) d\rho_0(y)}{\int q_\sigma(y|x) d\rho_0(y)}\| dx \leq t(C_8 \|z\|^2 + M_8) + t^2(C_9 \|z\|^4 + M_9) \quad (\text{B.25})$$

Using this result and  $\|\phi(z)\| \leq A\|z\| + B$  in (B.12), we finally obtain:



$$\begin{aligned}
& \left. \frac{d}{dt} \mathcal{E}(\hat{\rho}_t) - \frac{d}{dt} \mathcal{E}(\hat{\rho}_t) \right|_{t=0} \\
& \leq \frac{1}{\sigma^2} \int [t(C_8 \|z\|^2 + M_8) + t^2(C_9 \|z\|^4 + M_9)] \|\phi(z)\| d\rho_0(z) + \frac{t}{\sigma^2} \|\phi\|_{L^2(\rho_0)}^2 \\
& \leq t[Cm_3(\rho_0) + M] + t^2[Cm_5(\rho_0) + M]
\end{aligned} \tag{B.26}$$

The proof is complete. □

### B.1.2 Proof of main results

**Proposition B.4.** *Suppose Assumption 5.1, 5.2, 5.3, 5.4 hold. Then the following inequality holds for  $h < \frac{1}{A}$ :  $\mathcal{F}(\hat{\mu}_{(k+1)h}) - \mathcal{F}(\hat{\mu}_{kh}) \leq -\frac{1}{2}h \|\nabla_{W_2} \mathcal{F}(\mu_{kh})\|_{L^2(\mu_{kh})}^2 + \frac{1}{2}h\epsilon_k + h^2[Cm_3 + M] + h^3[Cm_5 + M]$ , where  $C, M$  are constants that do not relate to  $k$  or  $h$ .*

*Proof.* The KL divergence can be split into two terms:

$$\mathcal{F}(\hat{\mu}_t) := \int \log \frac{\hat{\mu}_t(x)}{\pi(x)} d\hat{\mu}_t(x) = \int -\log \pi(x) d\hat{\mu}_t(x) + \int \log \hat{\mu}_t(x) d\hat{\mu}_t(x) := \mathcal{G}(\hat{\mu}_t) + \mathcal{E}(\hat{\mu}_t) \tag{B.27}$$

Since

$$\mathcal{F}(\hat{\mu}_{(k+1)h}) - \mathcal{F}(\hat{\mu}_{kh}) = h \left. \frac{d}{dt} \right|_{t=0} \mathcal{F}(\hat{\mu}_{kh+t}) + \int_0^h \left[ \left. \frac{d}{dt} \right|_{t=t} \mathcal{F}(\hat{\mu}_{kh+t}) - \left. \frac{d}{dt} \right|_{t=0} \mathcal{F}(\hat{\mu}_{kh+t}) \right] dt \tag{B.28}$$

and

$$\left. \frac{d}{dt} \right|_{t=0} \mathcal{F}(\hat{\mu}_{kh+t}) = \langle \nabla_{W_2} \mathcal{F}(\mu_{kh}), v_{kh} \rangle_{\mu_{kh}} \leq -\frac{1}{2} \|\nabla_{W_2} \mathcal{F}(\mu_{kh})\|_{L^2(\mu_{kh})}^2 + \frac{1}{2} \epsilon_k \tag{B.29}$$

Set  $\phi = v_{kh}$ ,  $\rho_0 = \mu_{kh}$  and  $\rho_t = \mu_{kh+t}$  in Lemma B.2, we have

$$\left. \frac{d}{dt} \right|_{t=0} \mathcal{G}(\hat{\mu}_{kh+t}) - \left. \frac{d}{dt} \right|_{t=0} \mathcal{G}(\hat{\mu}_{kh+t}) \leq Lt \|\phi\|_{L^2(\hat{\mu}_{kh})}^2 \leq t(C_1 m_2 + M_1) \tag{B.30}$$

where  $m_2$  is the upper bound of the second moment of  $\mu_{kh}$ .

By Lemma B.3, we have

$$\left. \frac{d}{dt} \right|_{t=0} \mathcal{E}(\hat{\mu}_{kh+t}) - \left. \frac{d}{dt} \right|_{t=0} \mathcal{E}(\hat{\mu}_{kh+t}) \leq t[C_2 m_3 + M_2] + t^2[C_2 m_5 + M_2] \tag{B.31}$$

where  $m_3$  and  $m_5$  are the upper bounds of the third and fifth absolute moment of  $\mu_{kh}$ .

Note that  $\|z\|^3 + \frac{4}{27} \geq \|z\|^2$ , we have  $m_3 + \frac{4}{27} \geq m_2$ .

Then

$$\begin{aligned} & \int_0^h \left[ \frac{d}{dt} \mathcal{F}(\hat{\mu}_{kh+t}) - \frac{d}{dt} \bigg|_{t=0} \mathcal{F}(\hat{\mu}_{kh+t}) \right] dt \\ &= \int_0^h \left[ \frac{d}{dt} \mathcal{G}(\hat{\mu}_{kh+t}) - \frac{d}{dt} \bigg|_{t=0} \mathcal{G}(\hat{\mu}_{kh+t}) + \frac{d}{dt} \mathcal{E}(\hat{\mu}_{kh+t}) - \frac{d}{dt} \bigg|_{t=0} \mathcal{E}(\hat{\mu}_{kh+t}) \right] dt \\ &\leq h^2 [Cm_3 + M] + h^3 [Cm_5 + M] \end{aligned} \quad (\text{B.32})$$

Plug this back to (B.28) gives the desired result, the proof is complete.  $\square$

**Theorem B.5.** *Assume Proposition 5.5 holds, then the average of squared gradient norms satisfies  $\frac{1}{K} \sum_{k=1}^K \|\nabla_{W_2} \mathcal{F}(\mu_{kh})\|_{L^2(\mu_{kh})}^2 \leq \frac{R}{K^{\frac{1}{2}}} + \frac{S}{K^{\frac{2}{3}}} + \frac{1}{K} \sum_{k=1}^K \epsilon_k$  for  $K > \min\{\frac{A^2 \mathcal{F}(\hat{\mu}_0)}{Cm_3 + M}, \frac{A^3 \mathcal{F}(\hat{\mu}_0)}{Cm_5 + M}\}$ , where  $R := 4\sqrt{\mathcal{F}(\hat{\mu}_0)(Cm_3 + M)}$  and  $S := 4(\mathcal{F}(\hat{\mu}_0))^{\frac{2}{3}}(Cm_5 + M)^{\frac{1}{3}}$ .*

*Proof.* From Proposition 5.5 we have:

$$\mathcal{F}(\hat{\mu}_{(k+1)h}) - \mathcal{F}(\hat{\mu}_{kh}) \leq -\frac{1}{2}h \|\nabla_{W_2} \mathcal{F}(\mu_{kh})\|_{L^2(\mu_{kh})}^2 + \frac{1}{2}h\epsilon_k + h^2[Cm_3 + M] + h^3[Cm_5 + M] \quad (\text{B.33})$$

Take the sum from  $k = 0$  to  $k = K - 1$ , we obtain

$$\frac{1}{K} \sum_{k=1}^K \|\nabla_{W_2} \mathcal{F}(\mu_{kh})\|_{L^2(\mu_{kh})}^2 \leq \frac{2\mathcal{F}(\hat{\mu}_0)}{hK} + \frac{1}{K} \sum_{k=1}^K \epsilon_k + h(2(Cm_3 + M)) + h^2(2(Cm_5 + M)) \quad (\text{B.34})$$

Denote  $a = \frac{2\mathcal{F}(\hat{\mu}_0)}{K}$ ,  $b = 2(Cm_3 + M)$ ,  $c = 2(Cm_5 + M)$ , choose  $h = \min\{(\frac{a}{b})^{\frac{1}{2}}, (\frac{a}{c})^{\frac{1}{3}}\}$ , then choosing  $K > \min\{\frac{A^2 \mathcal{F}(\hat{\mu}_0)}{Cm_3 + M}, \frac{A^3 \mathcal{F}(\hat{\mu}_0)}{Cm_5 + M}\}$  leads to  $h < \frac{1}{A}$ . In this case, we have  $\frac{a}{h} + bh + ch^2 \leq 2((ab)^{\frac{1}{2}} + a^{\frac{2}{3}}c^{\frac{1}{3}})$ . Plugging back  $a, b, c$  gives the desired result.  $\square$

## B.2 Proof of Theorem 5.8

Consider ERM  $\hat{s} := \arg \min_{s \in \mathcal{S}} \frac{1}{n} \sum_{i=1}^n \ell(z_i; s)$ , where  $\ell(z; s) := \mathbb{E}_{q(x|z)} \|s(x) - \nabla \log q(x|z)\|^2$  and  $\{z_i\}$  are i.i.d. samples of  $\mu(z)$ . The population loss is given by  $\ell(s) := \mathbb{E}_{\mu(z)q(x|z)} \|s(x) - \nabla q(x|z)\|^2 =$

$\mathbb{E}_{\hat{\mu}(x)} \|s(x) - \nabla \log \hat{\mu}(x)\|^2 + c_*$ , where  $c_* = \mathbb{E}_{\mu(z)q(x|z)} \|\nabla \log \hat{\mu}(x) - \nabla \log q(x|z)\|^2$  is a constant independent of  $s$ .

*Proof.* Recall that  $\ell(z; s) = \mathbb{E}_{q(x|z)} \|s(x) - \nabla \log q(x|z)\|^2$ . Let  $R > 0$  be some constant defined later and the corresponding truncated loss  $\ell^{tr}(z; s) := \ell(z; s) \mathbb{1}_{\{\|z\|_\infty \leq R\}}$ . For any  $s \in \mathcal{S}, z \in \mathbb{R}^d$ , we have

$$\ell(z; s) \leq 2\mathbb{E}_{q(x|z)} [\|s(x)\|^2 + \|\nabla \log q(x|z)\|^2] \leq 2(M^2 + d/\sigma^2) =: b. \quad (\text{B.35})$$

For the minimizer of empirical score matching  $\hat{s}$ ,

$$\begin{aligned} \ell(\hat{s}) &= \mathbb{E}_{\mu(z)} \ell^{tr}(\hat{s}; z) + \mathbb{E}_{\mu(z)} \ell(\hat{s}; z) \mathbb{1}_{\{\|z\|_\infty > R\}} \\ &\leq \mathbb{E}_{\mu(z)} \ell^{tr}(\hat{s}; z) + \mathbb{P}(\|z\|_\infty > R) b \end{aligned} \quad (\text{B.36})$$

By Assumption 5.7,  $\mathbb{P}(\|z\|_\infty > R) \leq C \exp(-R^2/C)$  for some constant  $C$ . Hence with probability no less than  $1 - Cn \exp(-R^2/C)$ , for all  $1 \leq i \leq n$ , we have  $\|z_i\|_\infty \leq R$  and consequently  $\hat{s} = \arg \min_{s \in \mathcal{S}} \frac{1}{n} \sum_{i=1}^n \ell(z_i; s) = \arg \min_{s \in \mathcal{S}} \frac{1}{n} \sum_{i=1}^n \ell^{tr}(z_i; s) =: \arg \min_{s \in \mathcal{S}} \hat{\ell}^{tr}(s)$ .

Define the empirical Rademacher complexity of a function class  $\mathcal{F}$  as

$$\mathcal{R}_n(\mathcal{F}) := \mathbb{E}_\sigma \sup_{f \in \mathcal{F}} \left| \frac{1}{n} \sum_{i=1}^n \sigma_i f(z_i) \right|, \quad \sigma \sim \text{Unif}(\{-1, 1\}^n). \quad (\text{B.37})$$

For  $r > 0$ , let  $\mathcal{S}_r := \{s \in \mathcal{S} : \hat{\ell}^{tr}(s) \leq r\}$  and  $\mathcal{F}_r = \{\ell^{tr}(\cdot; s) : s \in \mathcal{S}_r\}$ . Note that for any  $f, g \in \mathcal{F}_r$ ,

$$\left\| \frac{1}{\sqrt{n}} \sum_{i=1}^n \sigma_i f(z_i) - \frac{1}{\sqrt{n}} \sum_{i=1}^n \sigma_i g(z_i) \right\|_{\psi_2} \lesssim \sqrt{\frac{1}{n} \sum_i \|f(z_i) - g(z_i)\|^2} \lesssim \|f - g\|_{L^2(\mathbb{P}_n)}. \quad (\text{B.38})$$

and  $\mathbf{diam}(\mathcal{F}_r, \|\cdot\|_{L^2(\mathbb{P}_n)}) \leq 2\sqrt{br}$ . Then by Dudley's bound [Srebro et al., 2010; Wainwright, 2019], we have

$$\mathcal{R}_n(\mathcal{F}_r) \lesssim \inf_{\alpha \geq 0} \left\{ \alpha + \int_\alpha^{2\sqrt{br}} \sqrt{\frac{\log \mathcal{N}(\mathcal{F}_r, \|\cdot\|_{L^2(\mathbb{P}_n)}, \varepsilon)}{n}} d\varepsilon \right\}. \quad (\text{B.39})$$

By Lemma B.6, for any  $K \geq 2R$  and  $\alpha_K := CM\sqrt{dr} \exp(-C'K^2/\sigma^2)$ ,

$$\begin{aligned} \mathcal{R}_n(\mathcal{F}_r) &\lesssim \inf_{\alpha \geq \alpha_K} \left\{ \alpha + \int_\alpha^{2\sqrt{br}} \sqrt{\frac{\log \mathcal{N}(\mathcal{F}_r, \|\cdot\|_{L^2(\mathbb{P}_n)}, \varepsilon)}{n}} d\varepsilon \right\} \\ &\lesssim \inf_{\alpha \geq \alpha_K} \left\{ \alpha + \int_\alpha^{2\sqrt{br}} \sqrt{\frac{\log \mathcal{N}(\mathcal{S}_r, \|\cdot\|_{L^\infty([-K, K]^d)}, \varepsilon/\sqrt{4r})}{n}} d\varepsilon \right\} \\ &\lesssim \inf_{\alpha \geq \alpha_K} \left\{ \alpha + \int_\alpha^{2\sqrt{br}} \sqrt{\frac{SL \log(LWKBr/\varepsilon)}{n}} d\varepsilon \right\} \\ &\lesssim \sqrt{\frac{brSL \log(LWKBr)}{n}} + \alpha_K. \end{aligned} \quad (\text{B.40})$$

Let  $K = \max \left\{ 2R, C\sigma \log^{\frac{1}{2}} \left( \frac{Mdn}{bSL} \right) \right\}$  and we finally obtain

$$\mathcal{R}_n(\mathcal{F}_r) \lesssim \sqrt{\frac{brSL \log(LWRB\sigma \log(dn))}{n}}. \quad (\text{B.41})$$

By [Bousquet \[2002, Theorem 6.1\]](#), with probability at least  $1 - \delta$ , for all  $s \in \mathcal{S}$ ,

$$\ell^{tr}(s) \leq \hat{\ell}^{tr}(s) + \mathcal{O} \left( \sqrt{\hat{\ell}^{tr}(s) \cdot \frac{\gamma_R + b \log(1/\delta)}{n}} + \frac{\gamma_R + b \log(1/\delta)}{n} \right), \quad (\text{B.42})$$

where  $\gamma_R = bSL \log(LWRB\sigma \log(dn))$ . Hence with probability no less than  $1 - Cn \exp(-R^2/C) - \delta$ , we have

$$\begin{aligned} \ell^{tr}(\hat{s}) &\leq \inf_{s \in \mathcal{S}} \ell^{tr}(s) + \mathcal{O} \left( \sqrt{\inf_{s \in \mathcal{S}} \ell^{tr}(s) \cdot \frac{\gamma_R + b \log(1/\delta)}{n}} + \frac{\gamma_R + b \log(1/\delta)}{n} \right) \\ &\leq \inf_{s \in \mathcal{S}} \ell(s) + \mathcal{O} \left( \sqrt{\inf_{s \in \mathcal{S}} \ell(s) \cdot \frac{\gamma_R + \log(1/\delta)}{n}} + \frac{\gamma_R + b \log(1/\delta)}{n} \right). \end{aligned} \quad (\text{B.43})$$

Combining it with [\(B.36\)](#) and defining  $R = C \log^{\frac{1}{2}}(n/\delta)$ , we conclude that with probability at least  $1 - 2\delta$ ,

$$\ell(s) \leq \inf_{s \in \mathcal{S}} \ell(s) + \mathcal{O} \left( \sqrt{\inf_{s \in \mathcal{S}} \ell(s) \cdot \frac{bSL \log(LWB\sigma \log(dn/\delta)) + b \log(1/\delta)}{n}} \right). \quad (\text{B.44})$$

Or equivalently,

$$\begin{aligned} \ell_{sm}(s) &\leq \inf_{s \in \mathcal{S}} \ell_{sm}(s) + \mathcal{O} \left( \sqrt{(\inf_{s \in \mathcal{S}} \ell_{sm}(s) + c_*) \cdot \frac{bSL \log(LWB\sigma \log(dn/\delta)) + b \log(1/\delta)}{n}} \right) \\ &\leq 2 \inf_{s \in \mathcal{S}} \ell_{sm}(s) + \mathcal{O} \left( \sqrt{c_* \cdot \frac{bSL \log(LWB\sigma \log(dn/\delta)) + b \log(1/\delta)}{n}} \right). \end{aligned} \quad (\text{B.45})$$

□

**Lemma B.6.** *There exists constants  $C, C' > 0$  such that, for any  $K \geq 2R, \varepsilon \geq C\sqrt{dr}M \exp(-C'K^2/\sigma^2)$ ,*

$$\mathcal{N}(\mathcal{F}_r, \|\cdot\|_{L^2(\mathbb{P}_n)}, \varepsilon) \leq \mathcal{N}(\mathcal{S}_r, \|\cdot\|_{L^\infty([-K, K]^d)}, \varepsilon/\sqrt{4r}) \quad (\text{B.46})$$

*Proof.* Given an  $(\varepsilon/\sqrt{4r})$ -net  $\{\{s_j\}_{j=1}^N\}$  in  $(\mathcal{S}_r, \|\cdot\|_{L^\infty([-K, K]^d)})$ , we aim to show that  $\{\ell^{tr}(\cdot; s_j)\}_{j=1}^N$  is an  $\varepsilon$ -net in  $(\mathcal{F}_r, \|\cdot\|_{L^2(\mathbb{P}_n)})$ . In fact, for any  $s \in \mathcal{S}_r$ , there exists  $s_j$  such that  $\|s_j - s\|_{L^\infty([-K, K]^d)} \leq$

$\varepsilon/\sqrt{4r}$ . Therefore, for any  $z \in [-R, R]^d$ ,

$$\begin{aligned}
\mathbb{E}_{q(x|z)} \|s(x) - s_j(x)\|^2 &\leq \mathbb{E}_{q(x|z)} \|s(x) - s_j(x)\|^2 \mathbb{1}_{\{\|x-z\|_\infty \leq K/2\}} + M^2 \mathbb{P}(\|x-z\|_\infty > K/2) \\
&\leq \|s - s_j\|_{L^\infty([-K, K]^d)}^2 + CdM^2 \exp(-K^2/C\sigma^2) \\
&\leq \varepsilon^2/4r + CdM^2 \exp(-C'K^2/\sigma^2) \\
&\leq \varepsilon^2/2r.
\end{aligned} \tag{B.47}$$

Note that in the second inequality we use  $K \geq 2R$  and probability of Gaussian-tail. Hence,

$$\begin{aligned}
\|\ell^{tr}(\cdot; s) - \ell^{tr}(\cdot; s_j)\|_{L^2(\mathbb{P}_n)} &\leq \sqrt{\frac{1}{n} \sum_{i=1}^n \left[ \mathbb{E}_{q(x|z_i)} (s(x) - s_j(x))^T (s(x) + s_j(x) - 2\nabla \log q(x|z_i)) \right]^2} \\
&\leq \sqrt{\frac{1}{n} \sum_{i=1}^n \mathbb{E}_{q(x|z_i)} \|s(x) - s_j(x)\|^2 \mathbb{E}_{q(x|z_i)} \|s(x) + s_j(x) - 2\nabla \log q(x|z_i)\|^2} \\
&\leq \sqrt{\varepsilon^2/2r \cdot 2r} = \varepsilon.
\end{aligned} \tag{B.48}$$

This concludes the proof.  $\square$

## C Additional Details of Experiments

### C.1 Gaussian Mixture

For the 2D experiment, the target marginal probability of each cluster is  $1/5$ , the mean of each cluster is randomly sampled from the standard gaussian distribution, the standard deviations of the clusters are 0.1, 0.2, 0.3, 0.4, 0.5. The initial distribution is the gaussian distribution  $\mathcal{N}((3, 0), 0.25\mathbf{I})$ . The number of particles is 1000.

For the neural network structure, we follow the setting of [Cheng et al. \[2023\]](#). For  $L_2$ -GF, Ada-GWG and Ada-SIFG, we parameterize  $f_\gamma$  as 3-layer neural networks with *tanh* activation function. Each hidden layer has 32 neurons. The inner loop iteration is 5 and we use SGD optimizer with Nesterov momentum (momentum 0.9) to train  $f_\gamma$  with learning rate  $\eta=1e-3$ . For  $L_2$ -GF and Ada-GWG, the particle step size is 0.1. For Ada-SIFG, the particle step size is 0.01.

For Ada-GWG, we set the initial exponent  $p_0 = 2$  and learning rate  $\tilde{\eta} = 5e-7$ . For Ada-SIFG, we set the initial noise magnitude  $\sigma_0 = 0.12$  and learning rate  $\hat{\eta} = 1e-9$ .

For the 10D experiment, the target marginal probability of each cluster is  $1/5$ , the mean of each cluster is randomly sampled from the standard gaussian distribution, the standard deviations of the clusters are 0.1, 0.2, 0.3, 0.4, 0.5. The initial distribution is the standard gaussian distribution. The

number of particles is 1000. The neural network structure is the same as which in the 2D Gaussian mixture experiment for  $L_2$ -GF, Ada-GWG, SIFG and Ada-SIFG. For  $L_2$ -GF and Ada-GWG, the particle step size is 0.1. For SIFG and Ada-SIFG, the particle step size is 0.01.

For Ada-GWG, we set the initial exponent  $p_0 = 2$  and learning rate  $\tilde{\eta} = 5e-7$ . For SIFG, we set the initial noise magnitude  $\sigma_0 = 0.1$ . For Ada-SIFG, we align with the initial noise magnitude  $\sigma_0 = 0.1$  of SIFG, and choose the learning rate  $\hat{\eta} = 1e-9$ .

We run the experiment on 5 random seeds. The average results and the variances are represented in the figure using lines and shades.

## C.2 Monomial Gamma

We follow the same setting as Cheng et al. [2023]. The number of particles is 1000. For  $L_2$ -GF and Ada-GWG, the neural network structure and its training optimizer are the same as which in the Gaussian mixture experiment. For all methods, the inner loop iteration is 5. For  $L_2$ -GF and Ada-GWG, we use Adam optimizer with learning rate  $\eta=1e-3$  to update the particles for better stability. For SIFG and Ada-SIFG, we use SGD optimizer with learning rate  $\eta=1e-2$ .

For Ada-GWG, we set the initial exponent  $p_0 = 2$  and learning rate  $\tilde{\eta} = 1$ . For SIFG, we set the initial noise magnitude  $\sigma_0 = 0.1$ . For Ada-SIFG, we align with the initial noise magnitude  $\sigma_0 = 0.1$  of SIFG, and choose the learning rate  $\hat{\eta} = 1e-10$ .

We run the experiment on 5 random seeds. The average results and the variances are represented in the figure using lines and shades.

## C.3 Independent Component Analysis

We follow the setting of Korba et al. [2021]. For  $L_2$ -GF, Ada-GWG, SIFG and Ada-SIFG, we parameterize  $f_\gamma$  as 3-layer neural networks with  $\tanh$  nonlinearities. Each hidden layer has 120 neurons. The inner loop  $N'$  is 20. We use SGD optimizer with learning rate  $\eta=1e-3$  to train  $f_\gamma$ . The particle step size is  $1e-3$ .

For Ada-GWG, we set the initial exponent  $p_0 = 2$  and learning rate  $\tilde{\eta} = 0.008$  (chosen from  $\{0.004, 0.008, 0.012\}$  for the best performance). We clip the exponent  $p$  within  $[1.1, 6]$ . The gradient of  $A(p)$  is also clipped within  $[-0.1, 0.1]$ .

For SIFG and Ada-SIFG, we set the initial noise magnitude  $\sigma_0 = 0.03$ . For Ada-SIFG, the learning rate for  $\sigma$  is  $2e-6$  (chosen from  $\{1e-6, 2e-6, 4e-6\}$  to obtain the best performance).

For SVGD, we use RBF kernel  $\exp(-\frac{\|x-y\|^2}{h})$  where  $h$  is the heuristic bandwidth [Liu and Wang, 2016]. For 10 particles, the particle step size is 1e-3 (chosen from {1e-2, 1e-3, 1e-4} to obtain the best performance). For 100 particles, the initial step size is 1e-1 (chosen from {5e-2, 1e-1, 2e-1} to obtain the best performance).

Additionally, we run standard HMC with step size 5e-4 for 10000 iterations as the ground truth for the posterior distribution.

## C.4 Bayesian Neural Networks

We follow the settings of Cheng et al. [2023]. For the UCI datasets, the datasets are randomly partitioned into 90% for training and 10% for testing. Then, we further split the training dataset by 10% to create a validation set for hyper-parameter selection as done in Cheng et al. [2023]. We select the step size of particle updates from {1e-4, 2e-4, 5e-4, 1e-3} for the best performance. For  $L_2$ -GF, Ada-GWG and Ada-SIFG, we parameterize  $f_\gamma$  as 3-layer neural networks. Each hidden layer has 300 neurons, and we use LeakyReLU as the activation function with a negative slope of 0.1. The inner loop  $N'$  is 10. We use the Adam optimizer and choose the learning rate from {1e-3, 1e-4} to train  $f_\gamma$ .

For Ada-GWG, we choose the initial exponent  $p_0$  to be 2 and set the learning rate  $\tilde{\eta}$  to be 1e-4. The gradient of  $A(p)$  is clipped within [-0.2, 0.2]. For Ada-SIFG, we choose the initial noise magnitude  $\sigma$  from {0.1, 0.01}. The learning rate for  $\sigma$  is chosen from {2e-5, 4e-5, 1e-4} for the best performance. For SVGD, we use the RBF kernel as done in [Liu and Wang, 2016]. For methods except SGLD, the iteration number is chosen to be 2000 to converge. For SGLD, the iteration number is set to 10000 to converge.